Constitutively active receptor ADGRA3 signaling induces adipose thermogenesis

Zewei Zhao[a], Longyun Hu[a], Bigui Song[a], Tao Jiang[a], Qian Wu[a], Jiejing Lin[a], Xiaoxiao Li[a], Yi Cai[a], Jin Li[a], Bingxiu Qian[a], Siqi Liu[a], Jilu Lang[b,] *, Zhonghan Yang[a,] *

[a]Shenzhen Key Laboratory of Systems Medicine for inflammatory diseases, School of Medicine, Shenzhen Campus of Sun Yat-Sen University, Sun Yat-Sen University, Shenzhen, 518107, Guangdong Province, China

[b]Department of Cardiovascular Surgery, Peking University Shenzhen Hospital, Shenzhen, 518107, Guangdong Province, China

*Corresponding authors (Zhonghan Yang, email: yangzhh@mail.sysu.edu.cn)

*Corresponding authors (Jilu Lang, email: langjl1983@126.com)

Running Head: ADGRA3 induces adipose thermogenesis

ABSTRACT

The induction of adipose thermogenesis plays a critical role in maintaining body temperature and improving metabolic homeostasis to combat obesity. β3-adrenoceptor (β3-AR) is widely recognized as a canonical β-adrenergic G protein-coupled receptor (GPCR) that plays a crucial role in mediating adipose thermogenesis in mice. Nonetheless, the limited expression of β3-AR in human adipocytes restricts its clinical application. The objective of this study was to identify a GPCR that is highly expressed in human adipocytes and to explore its potential involvement in adipose thermogenesis. Our research findings have demonstrated that the adhesion G protein-coupled receptor A3 (ADGRA3), an orphan GPCR, plays a significant role in adipose thermogenesis through its constitutively active effects. ADGRA3 exhibited high expression levels in human adipocytes and mouse brown fat. Furthermore, the knockdown of *Adgra3* resulted in an exacerbated obese phenotype and a reduction in the expression of thermogenic markers. Conversely, *Adgra3* overexpression activated the adipose thermogenic program and improved metabolic homeostasis without an exogenous ligand supplementation. We found that ADGRA3 facilitates the biogenesis of beige adipocytes through the Gs-PKA-CREB axis. Moreover, hesperetin was identified as a potential agonist of ADGRA3, capable of inducing adipocyte browning and ameliorating insulin resistance. In conclusion, our study demonstrated that the overexpression of constitutively active ADGRA3 or the activation of ADGRA3 by hesperetin can induce adipocyte browning by Gs-PKA-CREB axis. These findings indicate that the utilization of hesperetin and the selectively overexpression of ADGRA3 in adipose tissue could serve as promising therapeutic strategies in the fight against obesity.

Keywords: Obesity; Insulin resistance; Thermogenesis; ADGRA3; Hesperetin.

Introduction

Since 1975, there has been a substantial increase in the global prevalence of obesity, with the magnitude nearly tripling. The World Health Organization projects that the prevalence of obesity among adults will exceed 20% by the year 2025 (1). Currently, the management of excessive adiposity poses a paramount economic burden and healthcare predicament (2, 3). In addition to the detrimental social and psychological implications, a multitude of studies have consistently demonstrated a significant association between obesity and an increased vulnerability to a range of health conditions, such as type 2 diabetes, cardiovascular diseases, and cancer (4-7).

Activating and maintaining the thermogenesis of beige/brown fat has been shown to be effective in treating obesity and related metabolic disorders in humans (8, 9). As a well-established β-adrenergic GPCR, the β3-AR has been identified as a prominent target for stimulating adipose thermogenesis in mice. Regrettably, the clinical application of β3-AR has been impeded due to its low expression in human adipocytes and the cardiovascular risks associated with other adrenergic receptors (10, 11). G protein-coupled receptors (GPCRs) are the most prevalent class of drug targets among all drugs approved by the U.S. Food and Drug Administration (FDA). They also play a crucial role in the clinical treatment of obesity (12-14). Therefore, it is of clinical significance to identify novel GPCR targets that induce adipose thermogenesis.

ADGRA3 is classified as an orphan adhesion G protein-coupled receptor (aGPCR) and exhibits the typical domains found in aGPCRs within its N-terminal extracellular region (ECR), including a leucine-rich repeat (LRR), an immunoglobulin-like domain (Ig), a

hormone-binding domain (HBD), and a GAIN domain (15). ADGRA3 was initially discovered as a distinctive indicator of various spermatogonial progenitor cells (16, 17). Recent studies have shown that the orphan status of receptors has posed challenges to the study of aGPCRs. However, these studies have also uncovered a conservative mechanism of aGPCR activation, which involves the use of tethered ligands in the GAIN domain (18, 19). ADGRA3 has been previously identified as a receptor capable of auto-cleavage (20). However, the functional activity of ADGRA3 in a constructive manner is still uncertain. A genome-wide association study (GWAS) demonstrated a significant correlation between single nucleotide polymorphisms (SNPs) of ADGRA3 and body weight in chickens (21).

Nevertheless, the precise role of ADGRA3 in the progression of obesity and adipose thermogenesis remains uncertain. This study aimed to investigate three main aspects: (1) the impact of ADGRA3 on browning of white adipose tissue (WAT) and brown adipose tissue (BAT), (2) the effects of ADGRA3 on metabolic homeostasis, and (3) the underlying mechanisms by which ADGRA3 induces adipose thermogenesis.

Results

ADGRA3 is identified as a potential GPCR inducing the development of beige fat

We conducted a comprehensive analysis of three datasets to identify ADGRA3 as a potential GPCR target that promotes the development of beige fat (Figure 1A). To identify novel GPCRs that induce the biogenesis of beige fat, we conducted differential gene expression analysis (Figure 1B) and Venn diagram analysis (Figure 1C) using the GSE118849 dataset obtained from the Gene Expression Omnibus (GEO) database. Additionally, we

utilized the human subcutaneous adipocytes dataset (Figure 1C, red) and human visceral adipocytes dataset (Figure 1C, purple) from the human protein atlas database to obtain genes that are highly expressed in human white adipocytes. The GSE118849 dataset comprises samples of brown adipose tissue (BAT) and inguinal white adipose tissue (iWAT) obtained from mice subjected to a 72-hour cold exposure at a temperature of 4℃.

A total of 1134 differentially expressed genes (DEGs) that exhibited up-regulation in BAT compared to iWAT under cold stimulation were identified in the analysis, which might play a role in adipose thermogenesis. These DEGs were further screened to identify highly expressed GPCRs in BAT relative to WAT (Figure 1B, red). We conducted additional annotation on 1134 DEGs and identified that 27 of these genes were associated with the encoding of GPCRs (Supplementary File 2). Among the set of 27 genes, it was found that 24 genes were not present in the group of genes that exhibited high expression levels in human adipocytes, as determined by the human protein atlas database. Consequently, these 24 genes were excluded from further analysis. We conducted a comprehensive literature review and discovered that out of the three remaining GPCRs namely ADGRA3, ADRA1A, and ADRB1, only ADGRA3 has not been documented to have any association with brown fat. Therefore, our research subsequently shifted towards investigating the potential regulatory role of ADGRA3 in obesity and brown fat.

The findings indicated that the level of *Adgra3* expression in mouse adipose tissue (Figure 1D) was comparatively lower than that of *Adrb3*, the coding gene for β3-AR. Conversely, in human adipose tissue, *ADGRA3* expression was observed to be higher than that of *ADRB3* (Figures 1E and Figure 1-figure supplement 1E). We conducted an investigation to

examine the regulatory effects of a high-fat diet on the transcription of *Adgra3* and *Ucp1* (Uncoupling protein 1, a functional protein and marker of beige/brown fat). The findings of the study demonstrated that a HFD had a significant inhibitory effect on the expression of ADGRA3 and UCP1 in iWAT and BAT, while CL robustly increased the expression of ADGRA3 and UCP1 in iWAT and BAT (Figures 1F-G and Figure 1-figure supplement 1A-D). Interestingly, in human subcutaneous fat, there was a moderate positive correlation between the expression level of *ADGRA3* and the expression level of *UCP1* (R=0.5, Figure 1H). On the other hand, the expression level of *ADRB3* showed a weak positive correlation with the expression level of *UCP1* (R=0.21, Figure 1-figure supplement 1F). The data presented in this study indicate that ADGRA3 is a GPCR that exhibits high expression levels in BAT and may participate in inducing adipose thermogenesis.

Adgra3 overexpression induces the biogenesis of beige adipocytes in vitro

To ascertain the predominant expression of ADGRA3, the isolation of stromal Vascular Fraction (SVF) and mature adipocytes from WAT and BAT was conducted for subsequent validation. The results showed that ADGRA3 is predominantly expressed in adipocytes. Furthermore, the expression level of ADGRA3 in BAT adipocytes was found to be higher compared to WAT adipocytes (Figure 1I). However, no significant difference was observed in the expression level of ADGRA3 in the SVF of WAT and BAT (Figure 1I). Moreover, it was observed that the modulation of the expression levels of *Adgra3/ADGRA3* and *Ucp1/UCP1* exhibited a similar pattern during the differentiation process between mouse and human adipocytes (Figure 1-figure supplement 1G-H).

To investigate the role of ADGRA3 in the biogenesis of beige adipocytes, we conducted an experiment where we transformed pre-adipocytes 3T3-L1 into mature beige-like adipocytes with a knockdown of *Adgra3*. Our findings indicate that the knockdown of *Adgra3* resulted in a decrease in the expression of genes related to thermogenesis and lipolysis (Figure 2A). Western blot analysis and Mito-Tracker staining revealed a decrease in the expression of UCP1 (Figure 2B) and a reduction in the number of mitochondria (Figure 2C) following *Adgra3* knockdown. Lipid droplet fluorescence staining and intracellular triglyceride assay were performed on adipocytes to assess the impact of *Adgra3* knockdown. The results revealed a significant increase in the number of lipid droplets and intracellular triglyceride levels (Figures 2C-D) following *Adgra3* knockdown. Moreover, the uptake of 2-deoxy-D-glucose (2-NBDG), a fluorescently-labeled deoxyglucose analog, by adipocytes was significantly inhibited following the knockdown of *Adgra3* (Figure 2E). Furthermore, oxygen consumption rate (OCR) was detected to verify the effect of ADGRA3 on the oxygen consumption of adipocytes. The results indicated that the loss of ADGRA3 decreased the both basal and max OCR of adipocytes (Figures 2F-G).

Following the overexpression of *Adgra3*, there was an observed up-regulation in the expression of UCP1 in 3T3-L1 mature beige-like adipocytes (Figures 2H-I). Additionally, Mito-Tracker staining revealed an increase in the quantity of mitochondria (Figure 2J). There was a notable reduction observed in the lipid droplets and intracellular triglyceride levels (Figures 2J-K) subsequent to the overexpression of *Adgra3*. Moreover, the findings indicated that the overexpression of *Adgra3* resulted in an increased uptake of 2-NBDG by adipocytes (Figure 2L) and increased basal and maximum OCR (Figures 2M-N). The presented data

suggest that ADGRA3 has the ability to stimulate the formation of beige adipocytes in vitro.

Adgra3 knockdown suppresses adipose thermogenic program and impairs metabolic homeostasis in vivo

To evaluate the role of ADGRA3 in the biogenesis of beige fat in vivo, mice fed with a NCD were injected with shNC or sh*Adgra3* for 28 days (Figure 3A). After knocking down *Adgra3* in mice (Figure 3-figure supplement 1A-B), there was a significant increase in the weight of sh*Adgra3* mice (mice with *Adgra3* knockdown) (Figure 3B). Furthermore, the food intake of sh*Adgra3* mice was elevated slightly (Figure 3-figure supplement 1C). Serum triacylglycerol (TG) levels (Figure 3-figure supplement 1D), weight of iWAT, epididymal white adipose tissue (eWAT) and BAT (Figure 3C) were significantly higher in sh*Adgra3* mice. Liver weight (Figure 3C) and TG levels in the liver (Figure 3-figure supplement 1E) did not show a significant difference between shNC mice and sh*Adgra3* mice. Meanwhile, hematoxylin-eosin staining showed that *Adgra3* knockdown induced adipose expansion in iWAT (Figure 3-figure supplement 1F), eWAT (Figure 3-figure supplement 1G) and BAT (Figure 3-figure supplement 1F) but not lead to hepatic steatosis (Figure 3-figure supplement 1G).

Remarkably, the knockdown of *Adgra3* resulted in a significant reduction in both body temperature (Figure 3D) and BAT temperature (Figure 3E). Given the crucial influence of thyroid activity on thermogenesis, we measured the levels of serum free tetraiodothyronine (fT4) to evaluate the consequences of *Adgra3* knockdown on thyroid activity, which indicated that the nanoparticle-mediated *Adgra3* knockdown does not exert an inhibitory effect on

thyroid activity (Figure 3-figure supplement 1H). The knockdown of *Adgra3* resulted in a significant decrease in the expression of genes related to thermogenesis and lipolysis in both iWAT (Figure 3F) and BAT (Figure 3G). Moreover, the Western blot analysis (Figures 3H-I) and Immunohistochemical staining (Figure 3J) of UCP1 revealed comparable outcomes. Additionally, it was observed that the knockdown of *Adgra3* resulted in an increase in the size of lipid droplets and a decrease in the number of mitochondria in BAT (Figure 3K). Furthermore, nanomaterials carrying sh*Adgra3* were directly injected into BAT (Figure 3-figure supplement 1I), resulting in knockdown of *Adgra3* and down-regulation of thermogenic and lipolysis-related genes, as compared to BAT injected with shNC (Figure 3-figure supplement 1J). These findings indicate that ADGRA3 plays a crucial role as a receptor in the biogenesis of beige fat and the activation of BAT.

Moreover, the genes that were highly expressed in ADGRA3 high-expressed human subcutaneous adipose tissue (Figure 3-figure supplement 2A, red) exhibited enrichment in various biological processes. These processes included hyperinsulinism, obesity (Figure 3-figure supplement 2B), metabolic processes (Figure 3-figure supplement 2C), adipogenesis (Figure 3-figure supplement 2D), regulation of lipolysis in adipocytes (Figure 3-figure supplement 2E), and lipid metabolism (Figure 3-figure supplement 2F). GSEA was conducted to search the enriched KEGG pathways based on the expression level of ADGRA3 in human subcutaneous adipose dataset and human visceral adipose dataset from GTEx portal database. For ADGRA3 high-expressed group, both subcutaneous adipose dataset (Figure 3-figure supplement 2G) and visceral adipose dataset (Figure 3-figure supplement 2H) enriched in insulin signaling pathway, which indicates that ADGRA3 may be involved in the regulation of

glucose metabolism in addition to its influence on lipid metabolism. Furthermore, it was observed that sh*Adgra3* mice exhibited significant disruptions in overall glycemic homeostasis (Figure 3L) and insulin sensitivity (Figure 3M). Moreover, the fasting serum insulin level was increased and the homeostasis model assessment of insulin resistance (HOMA-IR) showed an increase in sh*Adgra3* mice (Figures 3N-O). Hence, the findings of this study provide evidence that the knockdown of *Adgra3* hampers adipose thermogenesis and disrupts metabolic homeostasis in vivo.

ADGRA3 activates the adipose thermogenic program and counteracts metabolic disease in vivo

To identify whether *Adgra3* overexpression induces adipose thermogenesis and improves the metabolic homeostasis against obesity, *Adgra3* OE and CON were injected i.p. into mice fed with a NCD (Figure 4-figure supplement 1A) and a HFD (Figure 4A), thereby establishing models of *Adgra3*-overexpressed mice (Figures 4F-G and Figure 4-figure supplement 1B-C). The growth of body weight of *Adgra3* OE mice was alleviated (Figure 4B) during the HFD feeding accompanied with a slight decrease of food intake (Figure 4-figure supplement 2A). Furthermore, the weight of iWAT, eWAT, BAT and liver (Figure 4C) were significantly decreased in *Adgra3* OE mice. The *Adgra3* OE mice exhibited an elevation in both body temperature (Figures 4D and Figure 4-figure supplement 1D) and BAT temperature (Figures 4E and Figure 4-figure supplement 1E), while there was no difference in serum fT4 levels (Figure 4-figure supplement 1F and Figure 4-figure supplement 2B). Meanwhile, *Adgra3* overexpression decreased the TG level in serum and liver (Figure 4-figure supplement

2C-D) as well as the area of adipocytes in iWAT, eWAT, BAT and liver (Figure 4-figure supplement 1G and Figure 4-figure supplement 2E-F).

Moreover, the expression levels of thermogenic and lipolysis-related genes were elevated in iWAT (Figures 4F and Figure 4-figure supplement 1H) and BAT (Figures 4G and Figure 4-figure supplement 1I). Western-blot (Figures 4H-I and Figure 4-figure supplement 1J-K) and immunohistochemical staining of UCP1 (Figures 4J and Figure 4-figure supplement 1L) showed that the expression of UCP1 was increased dramatically in iWAT and BAT after *Adgra3* overexpression. In addition, we found that after *Adgra3* overexpression, BAT presented multiple thermogenesis fat features (Figure 4K). Furthermore, nanomaterials carrying *Adgra3* OE were directly injected into BAT (Figure 4-figure supplement 2G), resulting in overexpression of *Adgra3* and upregulation of thermogenic and lipolysis-related genes, as compared to BAT injected with CON (Figure 4-figure supplement 2H). These findings indicate that the overexpression of *Adgra3* is capable of inducing the hallmarks of thermogenesis in mice, independently of other organs.

We then investigated the metabolic impact of ADGRA3. The glucose tolerance test (GTT) presented that *Adgra3* overexpression improved the glucose homeostasis of HFD mice (Figure 4L). The insulin tolerance test (ITT) showed that *Adgra3* overexpression alleviated the insulin resistance of HFD mice (Figure 4M). Moreover, the fasting serum insulin level was reduced after *Adgra3* overexpression (Figure 4N) and the HOMA-IR also showed a robust improvement (Figure 4O) in *Adgra3*OE mice. Taken together, *Adgra3* overexpression activates the adipose thermogenic program and improves the metabolic homeostasis in diet-induced obese mice against obesity and insulin resistance in vivo.

ADGRA3 activates the adipose thermogenic program via the G_s-PKA-CREB axis

To ascertain the ADGRA3-conjugated Gα protein, we conducted an overexpression of FLAG-labeled mouse ADGRA3 and four different types of His-labeled G_α proteins (G_s, G_i, G_q and G_{12}) in 293T cells. The lysate obtained from the 293T cells was then utilized for the subsequent co-immunoprecipitation (co-IP) analysis. The results of the co-IP experiment demonstrated that mouse ADGRA3 coupled to the G_s protein (Figures 5A-B), while no interaction was observed with the other three Gα proteins (G_i, G_q and G_{12}; Figure 5-figure supplement 1A-C) ADGRA3 exhibits intrinsic and auto-cleavable receptor activity, allowing it to signal even in the absence of an exogenous ligand (16, 20). Hence, the overexpression of *Adgra3* is capable of inducing cAMP production (Figure 5C), which serves as a second messenger indicating the activation of downstream signals mediated by G_s protein. This response is comparable to the effect of a ligand. However, there is no production of IP1, which is a metabolite of the downstream second messenger IP3 associated with G_q protein (Figure 5-figure supplement 1D). Additionally, our findings indicate that the effect of *Adgra3* overexpression on cAMP production is dependent on G_s protein (Figures 5D and Figure 5-figure supplement 1E). These results suggest that ADGRA3 is involved in the coupling of G_s protein, leading to the stimulation of downstream cAMP production.

Hence, it was hypothesized that the overexpression of *Adgra3* could potentially stimulate adipocyte thermogenesis by activating the PKA signaling pathway. As expected, the Western-blot analysis revealed that the overexpression of *Adgra3* leads to an elevation in the phosphorylated form of CREB (p-CREB), indicating an increase in PKA-CREB signaling

activity. This effect was observed in 3T3-L1 (Figure 5E), as well as in the iWAT and BAT (Figure 5F). Consistently, the knockdown of *Adgra3* resulted in a decrease in the level of p-CREB in 3T3-L1 (Figure 5G), as well as in iWAT and BAT (Figure 5H). To investigate the potential role of *Adgra3* overexpression in promoting the biogenesis of beige adipocytes and activating the PKA-CREB signaling pathway via G_s protein, we conducted an experiment using 3T3-L1 cells. The cells were treated with *Adgra3* OE and sh*Gnas*, respectively. *Adgra3* overexpression was found to be adequate in inducing the expression of UCP1 in 3T3-L1 cells. However, this effect was observed to be eliminated when *Gnas* was knocked down (Figure 5I and Figure 5-figure supplement 1E). Furthermore, the utilization of PKAi (protein kinase A inhibitor, H-89) was employed to ascertain the dependence of the browning effect of Adgra3 overexpression on the PKA-CREB signal. The results showed that PKAi effectively inhibited the activation of PKA-CREB signaling and UCP1 expression induced by *Adgra3* overexpression (Figures 5J and Figure 5-figure supplement 1F). These results suggest that the observed browning effect resulting from *Adgra3* overexpression is mediated through the PKA-CREB signaling pathway. Collectively, these findings indicate that ADGRA3 facilitates the biogenesis of beige adipocytes through the G_s-PKA-CREB signaling pathway.

Hesperetin: a screened ADGRA3 agonist that induces the biogenesis of beige adipocytes

Considering the difficulty of overexpressing ADGRA3 in clinical application, hesperetin was screened as a potential agonist of ADGRA3 by PRESTO-Salsa database (Figure 6A). The results showed that hesperetin treatment stimulates cAMP production (Figure 6B) and increases the expression level of UCP1 and p-CREB (Figures 6C-D). To verify whether

hesperetin induces the biogenesis of beige adipocyte and activates PKA-CREB signal via ADGRA3, we treated 3T3-L1 with hesperetin and sh*Adgra3*, respectively. We found that the induction effect of hesperetin on UCP1 and p-CREB is eliminated when *Adgra3* is knocked down (Figures 6E-F). In addition, OCR was detected to verify the effect of hesperetin on the oxygen consumption of adipocytes. The results indicated that hesperetin increased the both basal and max OCR of adipocytes, which was ADGRA3-dependent (Figures 6G-H).

Moreover, the results showed that the induction effect of hesperetin on UCP1 and p-CREB is attenuated after *Gnas* knocked down (Figures 6I-J), suggesting that hesperetin up-regulates UCP1 and activates PKA-CREB axis dependent on G_s. Furthermore, PKAi was used to verify whether the browning effect of hesperetin was dependent on PKA-CREB signal. The results revealed that hesperetin treatment resulted in the upregulation of UCP1 and p-CREB. However, this effect was found to be eliminated when PKAi was applied (Figures 6K-L), suggesting that the induction of UCP1 and p-CREB by hesperetin is dependent on PKA. These findings suggest that hesperetin exerts an induction effect on biogenesis of beige adipocytes via ADGRA3-G_s-PKA-CREB axis.

Hesperetin: a potential ADGRA3 agonist that activates the adipose thermogenic program and counteracts metabolic disease dependent on ADGRA3

To identify whether hesperetin induces adipose thermogenesis and improves the metabolic homeostasis against obesity via ADGRA3, shNC mice or sh*Adgra3* mice were treated with hesperetin and fed with a HFD (Figure 7A). Hesperetin was found to alleviate the growth of body weight (Figure 7B) during the HFD feeding and the weight of iWAT, eWAT,

BAT and liver weight ratio (Figure 7C), which was dependent on ADGRA3. It is noteworthy that the food consumption of sh*Adgra3* mice slightly surpassed that of shNC mice, while the administration of hesperetin remained uninfluential on their dietary intake (Figure 7-figure supplement 1A). Hesperetin increased body temperature (Figure 7D) and BAT temperature (Figure 7E) in shNC mice, which were significantly blunted in sh*Adgra3* mice. The levels of serum fT4 were measured to evaluate the consequences of hesperetin treatment on thyroid activity, which indicated that hesperetin treatment does not activate thyroid activity (Figure Figure 7-figure supplement 1B).

Concurrently, hesperetin induced a decline in TG level in both serum (Figure 7-figure supplement 1C) and liver (Figure 7-figure supplement 1D), and also reduced the area of adipocytes in iWAT (Figure 7-figure supplement 1E) and BAT (Figure 7-figure supplement 1F). However, these effects were absent in sh*Adgra3* mice. Moreover, the expression level of UCP1 were elevated in both iWAT (Figures 7F and 7H) and BAT (Figures 7G and 7I) after hesperetin treatment in shNC mice but not in sh*Adgra3* mice. The results indicated that hesperetin treatment resulted in a substantial decrease in lipid droplet size and a significant increase in mitochondria quantity in BAT (Figure 7J). However, this browning effect was weakened in sh*Adgra3* mice. These findings suggest that hesperetin is sufficient to orchestrate the hallmarks of thermogenesis in mice, which is dependent on ADGRA3.

We then investigated the metabolic impact of hesperetin treatment. The GTT presented that hesperetin improved the glucose resistance of HFD mice which showed no effect in sh*Adgra3* mice (Figure 7K). The ITT showed that hesperetin alleviated the insulin resistance of HFD mice which showed no significance in sh*Adgra3* mice (Figure 7L). Moreover, the

fasting serum insulin level was reduced after hesperetin treatment (Figure 7M) and the HOMA-IR also showed a moderate improvement (Figure 7N), which were dependent on ADGRA3. Taken together, hesperetin activates the adipose thermogenic program and improves the metabolic homeostasis in diet-induced obese mice against obesity and insulin resistance in vivo, which is ADGRA3 dependent.

ADGRA3 overexpression induces the biogenesis of human beige adipocytes in vitro

Given the elevated expression level of *ADGRA3* compared to *ADRB3* in human adipose tissue (Figures 1E and Figure 1-figure supplement 1E), we induced human adipose-derived mesenchymal stem cells (hADSCs) and mouse adipose-derived stromal vascular fraction (SVF) into adipocytes to evaluate the effect of ADGRA3 on human adipocytes. The results showed that *ADGRA3* knockdown led to a diminished expression of *UCP1* (Figure 8A and 8E), whereas its overexpression elicited an enhancement in *UCP1* expression (Figure 8B and 8F). Furthermore, Mito-Tracker and lipid droplet fluorescence staining illuminated a notable increase in lipid droplet count accompanied by a decrease in mitochondrial number following *ADGRA3* knockdown (Figure 8C). Conversely, *ADGRA3* overexpression resulted in a visible surge in mitochondrial quantity and a marked reduction in lipid droplet presence (Figure 8D). To further verify whether hesperetin induces the expression of UCP1 via ADGRA3, we treated mouse primary adipocytes with hesperetin and sh*Adgra3*, respectively. We found that the induction effect of hesperetin on UCP1 is eliminated when *Adgra3* is knocked down (Figures 8G-H) in primary cultures.

Discussion

In the present study, we have elucidated a novel role of ADGRA3 and hesperetin in inducing the development of beige adipocytes through the activation of the G_s-PKA-CREB signaling pathway. ADGRA3 is responsible for the activation of the adipose thermogenic program and plays a significant role in maintaining systemic glucose homeostasis. Additionally, the development of beige adipocytes induced by hesperetin is contingent upon the presence of ADGRA3. The novelty of this study is the discovery that ADGRA3 plays a role in the advancement of beige fat and the regulation of metabolic homeostasis. This suggests that targeting the ADGRA3-G_s-PKA-CREB signaling pathway could potentially be a therapeutic approach for obesity and related metabolic disorders.

The induction of beige fat has been investigated as a potentially effective therapeutic approach in combating obesity (22). A clinical trial revealed that treatment with the chronic β3-AR agonist mirabegron leads to an increase in human brown fat, HDL cholesterol, and insulin sensitivity (23). Subsequently, Blondin et al discovered that oral administration of mirabegron only elicits an increase in BAT thermogenesis when administered at the maximal allowable dose, indicating that human brown adipocyte thermogenesis is primarily driven by β2-adrenoceptor (β2-AR) stimulation (11). Consistent with this finding, we found much higher levels of ADRB2 expression in human white adipose tissue than ADRB3 (Figure 1-figure supplement 1E). Furthermore, a recent study has demonstrated that simultaneous activation of β2-AR and β3-AR enhances whole-body metabolism through beneficial effects on skeletal muscle and BAT (24).

While the promotion of thermogenesis in brown and beige adipocytes in rodents was

effectively achieved by the β3-adrenoceptor agonist, the clinical implications of this finding appear to be unfeasible in humans due to the low efficacy of β3-adrenoceptor agonists (25, 26). It is of utmost importance to investigate alternative therapeutic targets that can effectively and selectively enhance beige adipogenesis in order to combat obesity and its related metabolic disorders. In this study, we have identified ADGRA3 as a novel GPCR therapeutic target that exhibits high expression in human adipocytes. In human adipose tissue, ADGRA3 is expressed at a lower level than ADRB2 (Figure 1-figure supplement 1 E), which has been shown to be the main receptor mediating adrenergic activation of thermogenesis in human brown adipocytes (11). Nevertheless, given ADRB2's pivotal role in bronchodilation and vasodilation (27, 28), we believe that ADGRA3 has the potential to be an alternative target for inducing adipose thermogenesis. Overall, these findings suggest that ADGRA3, when overexpressed or stimulated by its potential agonist, hesperetin, can induce the biogenesis of beige fat.

Hesperetin has been reported to attenuate the age-related metabolic decline, reduce fat and improve glucose homeostasis in naturally aged mice (29). Previous studies showed that hesperetin improved glycemic control (29, 30) and was involved in adipocyte differentiation (31), but whether hesperetin induces the biogenesis of beige adipocyte was uncertain. Previously, the influence of hesperetin on ADGRA3 has remained unreported. In this study, we screened hesperetin as a potential agonist for ADGRA3 by using the PRESTO-Salsa tool as well as discovered that hesperetin has an agonist effect on ADGRA3 through a series of experiments. This study focuses on the regulatory effect of hesperetin on adipose thermogenesis and explores whether this effect is dependent upon ADGRA3. As such, we

refrained from conducting further investigations into other potential effects of hesperidin, including its potential role in antioxidant and in apoptosis.

In previous reports, male mice deficient in ADGRA3 showed obstructive azoospermia with high penetrance (15). Moreover, a genome-wide association study (GWAS) identified a single nucleotide polymorphism (SNP) located in the downstream region of *ADGRA3* as a genomic locus associated with body weight in chickens, suggesting that the ADGRA3 is a potential regulator of body weight (21). Nevertheless, the agonist and the downstream signal axis of ADGRA3 remain unclear as well as the effects of ADGRA3 on adipose thermogenesis and glucose homeostasis have not been explored. Consequently, our study has confirmed that the knockdown of *Adgra3* exacerbates obesity and disrupts glucose homeostasis. Additionally, both the overexpression of *Adgra3* and the administration of hesperetin have been found to stimulate the biogenesis of beige adipocytes through the ADGRA3-G_s-PKA-CREB signaling pathway and improve glucose homeostasis.

Given the consideration that the non-targeted nanoparticle approach utilized in this study for modulating *Adgra3* expression levels in vivo alter *Adgra3* expression in tissues beyond adipose tissue (Figure 3-figure supplement 1A-B and Figure 4-figure supplement 1B-C), notably the liver and skeletal muscle, the construction of *Adgra3* adipose tissue-specific knockout/overexpression mouse models is imperative for a more nuanced understanding of the precise mechanisms underlying the influence of on adipose thermogenesis. Furthermore, it is crucial to highlight that the observed decrease in TG levels in both serum and liver (Figure 4-figure supplement 2C-D) might be attributed to the significant increase in *Adgra3* expression in the liver, which is a consequence of the nanoparticle-mediated overexpression

of *Adgra3*. While the exact mechanism remains to be fully elucidated, this correlation suggests a potential link between *Adgra3* overexpression in the liver and reduced TG levels in the serum. We will employ more sophisticated models in subsequent studies to further elucidate the effects of ADGRA3 on adipose thermogenesis and metabolic homeostasis. Nevertheless, our findings underlie a potential therapeutic feature of ADGRA3 and hesperetin in obesity and the associated metabolic diseases from the thermogenic viewpoint of beige fat.

In conclusion, the activation of the G_s-PKA-CREB axis by ADGRA3 has been found to induce adipose thermogenesis, promote lipid metabolism, and alleviate lipid accumulation in adipose tissues (Figure 9). Furthermore, the induction of beige adipocyte biogenesis by hesperetin occurs through the ADGRA3-G_s-PKA-CREB axis. Given the importance of identifying signaling pathways that induce beige fat and alleviate obesity-related dysfunction in adipose tissue, our research findings suggest that hesperetin and activation of the intracellular signaling of ADGRA3 could serve as a promising and innovative therapeutic approach.

Materials and methods

Nanomaterials

The nanomaterials mentioned in this article refer to Lipo8000 reagent (Beyotime, C0533), a highly efficient transfection reagent based on nanomaterials, unless otherwise specified.

Mice

Wild-type (WT) C57BL/6J mice were obtained from the Center of Laboratory Animal at

Sun Yat-sen University. All mice were housed in the Sun Yat-sen University Laboratory Animal Center, where they were subjected to a 12-hour light-dark cycle and maintained at a controlled environmental temperature of 21±1℃. Eight-week-old male C57BL/6J mice were fed with a normal chow diet (NCD) or a high fat diet (HFD, 60% kcal) for 12 weeks to render mice obese. With the exception of mice fed with a HFD, male mice at the age of eight weeks were utilized in all experimental procedures.

For the knockdown and over-expression experiments of *Adgra3* in mice fed with a NCD, the following procedures were conducted: sh*Adgra3* (pLKO.1-U6-sh*Adgra3*-2 plasmid encapsulated in nanomaterials) and shNC (pLKO.1-U6-shNC plasmid encapsulated in nanomaterials) were injected intraperitoneally (i.p.) for knockdown experiments, while *Adgra3* OE (pLV3-CMV-*Adgra3* (mouse)-3×FLAG plasmid encapsulated in nanomaterials) and CON (pLV3-CMV-MCS-3×FLAG plasmid encapsulated in nanomaterials) were injected i.p. for over-expression experiments. The frequency of the sessions was twice a week over a period of four weeks. For the knockdown and over-expression experiments of *Adgra3* in mice fed with a HFD, the following procedures were conducted: sh*Adgra3* and shNC were injected intraperitoneally (i.p.) for knockdown experiments, while *Adgra3* OE and CON were injected i.p. for over-expression experiments. The frequency of the sessions was twice a week over a period of 12 weeks. For the local over-expression or knockdown of *Adgra3* in BAT of mice fed with a NCD, *Adgra3* OE, sh*Adgra3*, CON and shNC were injected locally into BAT once.

For the treatment with a selective β3-adrenoceptor agonist, CL-316,243 (hereafter referred to as CL), mice fed a HFD were injected intraperitoneally (i.p.) with CL (1 mg/kg daily) for 7 days. For the treatment with hesperetin (Hes), hesperetin is dissolved in drinking

water (200mg/L) and water were available ad libitum.

Intraperitoneal injections of glucose (2g/kg for mice fed with a NCD and 1g/kg for mice fed with a HFD) or insulin (0.5U/kg for mice fed with a NCD and 1U/kg for mice fed with a HFD) were administered. At the designated time points of 0 minutes, intraperitoneal glucose or insulin tolerance tests were conducted on mice that had been fasted for six hours. After administration, the blood glucose concentration was assessed at specific time intervals using a OneTouch Ultra Glucometer. Finally, the animals were euthanized, followed by the collection of tissue samples. Cohorts of ≥3 mice per genotype or treatment were assembled for all in vivo studies. All in vivo studies were repeated 2-3 independent times. All procedures related to animal feeding, treatment and welfare were conducted at Sun Yat-sen University Laboratory Animal Center. All the animal experiments were conducted with the approval of the Animal Care and Use Committee of Sun Yat-sen University (Approval ID: SYSU-IACUC-MED-2023-B082). This study was conducted in accordance with the ethical principles derived from the Declaration of Helsinki and Belmont Report and was approved by the review board of Sun Yat-sen University (Guangzhou, China).

Stromal Vascular Fraction (SVF) and mature adipocytes isolation

SVF from inguinal white adipose tissue (iWAT) and BAT of WT male mice at 4 weeks of age were washed with PBS, minced and digested with 0.1% type II collagenase in Dulbecco's modified eagle medium (DMEM) containing 3% BSA and 25μg/ml DNase I for 30 min at 37°C. During the digestion, the mixed solution was shaken by a hand every 5 min. The mixed solution was filtered through a 70 μm cell strainer and then centrifuged at 500 g for 5 min at

4℃. The floating mature adipocytes were collected for subsequent analysis, and the pellets containing SVF were resuspended in red blood cell lysis buffer for 5 min at 37℃. Cells were centrifuged at 500 g for 10 min at 4℃ and the SVF pellets were collected for subsequent analysis.

Cell culture

3T3-L1 and 293T cell lines were purchased from the Cell Bank of the Chinese Academy of Sciences in Shanghai, and both were identified by STR and tested negative for mycoplasma. Human adipose-derived mesenchymal stem cells (hADSCs) were purchased from the National Stem Cell Translational Resource Center. 3T3-L1 cells were culture and grown to confluence in high-glucose DMEM supplemented with 10% newborn calf serum (NCS). 293T cells were culture and grown to confluence in high-glucose DMEM supplemented with 10% FBS. Confluent 3T3-L1 and SVF pre-adipocytes were induced into mature beige-like adipocytes with 0.5 mM isobutyl methylxanthine (IBMX), 1 μM dexamethasone, 5 μg/ml insulin, 1 nM 3, 3', 5-Triiodo-L-thyronine (T3), 125 μM indomethacin and 1 μM rosiglitazone in high-glucose DMEM containing 10% FBS for 2 days, then treated with high-glucose DMEM containing 5 μg/ml insulin, 1 nM T3, 1 μM rosiglitazone and 10% FBS for 6 days and cultured with high-glucose DMEM containing 10% FBS for 2 days. hADSCs were seeded on plates coated with 0.1% gelatin and culture and grown to confluence in human mesenchymal stem cells (hMSCs) specialized culture medium (ZQ-1320). Confluent hADSCs were induced into mature human adipocytes with adipogenic induction medium (PCM-I-004) according to the manufacturer’s instructions.

The sh*Adgra3*, sh*Gnas* (pLKO.1-U6-sh*Gnas* plasmid encapsulated in nanomaterials) and

shNC were added to 3T3-L1 mature beige-like adipocytes for 72 hours. The sh*ADGRA3* (pLKO.1-U6-sh*ADGRA3*-(1/2/3) plasmid encapsulated in nanomaterials) and shNC were added to human adipocytes for 72 hours. The pcDNA3.1(+)-m*Gnas*-6×His (mixture of pcDNA3.1(+)-*Gnas*(mouse)-6×His plasmid and transfection reagent), pcDNA3.1(+)-m*Gnai1*-6×His (mixture of pcDNA3.1(+)-*Gnai1*(mouse)-6×His plasmid and transfection reagent), pcDNA3.1(+)-m*Gnaq*-6×His (mixture of pcDNA3.1(+)-*Gnaq*(mouse)-6×His plasmid and transfection reagent), pcDNA3.1(+)-m*Gna12*-6×His (mixture of pcDNA3.1(+)-*Gna12*(mouse)-6×His plasmid and transfection reagent), *Adgra3* OE and CON were added to 3T3-L1 mature beige-like adipocytes or 293T for 48 hours. The *ADGRA3* OE (pLV3-CMV-*ADGRA3*(human)-3×FLAG plasmid encapsulated in nanomaterials) and CON were added to human adipocytes for 48 hours. Hesperetin (10 μM) and PKAi (protein kinase A inhibitor, 20 μM H-89) was added to 3T3-L1 mature beige-like adipocytes for 48 hours. All in vitro studies were repeated 2-3 independent times.

Construction of plasmid

The pLV3-CMV-*Adgra3*(mouse)-3×FLAG, pLV3-CMV-*ADGRA3*(human)-3×FLAG, pLKO.1-U6-sh*ADGRA3*-(1/2/3), pLV3-CMV-MCS-3×FLAG, pcDNA3.1(+)-*Gnas*(mouse)-6×His, pcDNA3.1(+)-*Gnai1*(mouse)-6×His, pcDNA3.1(+)-*Gnaq*(mouse)-6×His and pcDNA3.1(+)-*Gna12*(mouse)-6×His plasmids were purchased from Shenzhen Yanming Biotechnology Co., LTD. The pLKO.1-U6-sh*Adgra3*-(1/2/3) and pLKO.1-U6-shNC plasmids were purchased from Guangzhou Hanyi Biotechnology Co., LTD.

Temperature measurements

The body temperature was measured at 9:00 using a rectal probe connected to a digital

thermometer.

Real-time Polymerase Chain Reaction (PCR)

Total RNA from tissue or cells was extracted with Trizol reagent. RNA concentration was measured by a NanoDrop spectrometer. 1000ng total RNA was reverse transcribed into cDNA by All-in-One RT SuperMix (G3337). Real-time PCR analysis using SYBR-Green fluorescent dye was performed with Step One Plus RT PCR System. Primers used for real-time PCR were listed in Supplementary File 1.

Histology and immunohistochemistry

Subcutaneous, epididymal white adipose tissue, interscapular brown adipose tissue and liver were fixed in 4% paraformaldehyde. Tissues were embedded with paraffin and sectioned by microtome. The slides were stained with hematoxylin and eosin (HE) using a standard protocol. For UCP1 and ADGRA3 immunohistochemistry, slides of various tissue were blocked with goat serum for 1h. Subsequently, the slides were incubated with anti-UCP1 (1:1000; ab10983) or anti-ADGRA3 (1:200; 11912-1-AP) overnight at 4℃ followed by detection with the EnVision Detection Systems. Hematoxylin was used as counterstain.

Western-blot

Tissues and cells were lysed in RIPA buffer supplemented with 1 mM PMSF and protease inhibitor cocktail (K1007). The protein concentration was measured by the BCA protein assay kit (BL521), and total cellular protein (25 μg) was subject to Western-blot analysis. The protein transferred to the PVDF membrane was probed with primary antibodies specific for HSP90 (1:1000; C45G), α-tubulin (1:10000; 666031-1-Ig), ADGRA3 (1:1000; 11912-1-AP), UCP1 (1:1000 for iWAT and cells or 1:10000 for brown adipose tissue (BAT);

ab10983), FLAG-tag (HRP Conjugated, 1:2000; AF2855), HIS-tag (HRP Conjugated, 1:2000; AF2879), p-CREB (1:1000; AF5785) and CREB (1:1000; AF6566) overnight at 4 °C. Except FLAG-tag protein and HIS-tag protein, after being incubated with HRP conjugated secondary antibody, proteins were detected with chemiluminescence using Immobilon Western HRP Substrate on ChemiDoc MP Imaging System. The ImageJ software was used for gray scanning. For all Western-blots, each lane represented an independent sample and all experiments were replicated 2 to 3 times.

IP assay

HEK293T cells were transfected using PEI 40K transfection reagent (G1802) with indicated cDNAs and cultured using the manufacture's protocol. Cells were lysed with IP lysis buffer (G2038) containing protease inhibitor cocktail (K1007). The lysates were precipitated with the FLAG-tag antibody (GB15938) or HIS-tag antibody (GB151251) in the presence of protein A+G agarose (P2055). The precipitants were washed five times with the IP lysis buffer and analyzed by immunoblot with the indicated antibodies.

Enzyme-linked immunosorbent assay (ELISA)

Mouse cAMP level was detected using a sensitive ELISA kit (MM-0544M2) purchased from Jiangsu Meimian Industrial Co., Ltd. Mouse IP1 level was detected using a sensitive ELISA kit (MM-0790M2) purchased from Jiangsu Meimian Industrial Co., Ltd. Mouse insulin level was detected using a sensitive ELISA kit (MM-0579M1) purchased from Jiangsu Meimian Industrial Co., Ltd. Mouse free tetraiodothyronine (fT4) level was detected using a sensitive ELISA kit (RXJ202449M) purchased from Quanzhou Ruixin Biological Technology Co., Ltd. All measurements were performed using the manufacture's protocol.

Bodipy staining

For the lipid staining, the differentiated adipocytes were washed twice with PBS. The cells were then stained with 2 μM BODIPY staining solution (GC42959) for 15 min at 37℃, then washed three times with PBS according to manufacturer's instructions. The stained cells were observed using a fluorescence microscope.

Mito-Tracker staining

The differentiated adipocytes were incubated with 100nM Mito-Tracker Red CMXRos (C1049) for 30 min according to manufacturer's instructions. Then cells were washed with PBS and visualized under the confocal microscope.

Determination of 2-deoxy-D-glucose (2-NBDG) uptake

The differentiated adipocytes were washed twice with PBS. The cells were then incubated with 100 μM 2-NBDG staining solution (HY-116215) for 30 min at 37℃, then washed three times with PBS. The stained cells were observed using a fluorescence microscope.

Measurement of Triacylglycerol (TG)

The triacylglycerol in adipocytes, tissues and plasma was measured by using Triglyceride Assay Kit (A110-1-1) according to the manufacturer’s instructions.

Transmission electron microscopy

BAT sections were fixed in 2% (vol/vol) glutaraldehyde in 100mM phosphate buffer, pH 7.2 for 12 h at 4℃. The sections were then post-fixed in 1% osmium tetroxide, dehydrated in ascending gradations of ethanol and embedded in fresh epoxy resin 618. Ultra-thin sections (60-80 nm) were cut and stained with lead citrate before being examined on the FEI-Tecnai

G2 Spirit Twin transmission electron microscope.

Differential expression analysis

The R package Linear Models for Microarray Data (limma) was used to analyze differential RNA-Sequencing expression. For screening high-expressed G-protein-coupled receptors in mouse BAT, limma was applied in the GSE118849 dataset to screen out BAT-elevated genes. For screening ADGRA3 high-expressed gene sets in human subcutaneous adipose, limma was applied in the human subcutaneous adipose dataset from GTEx Portal to screen out ADGRA3 high-expressed gene sets. Genes highly expressed in human adipocytes were obtained from the human protein atlas database. Genes with the cutoff criteria of $|\log FC| \geq 1.0$ and $P < 0.05$ were regarded as differentially expressed genes (DEGs). The DEGs of the GSE118849 dataset and the human subcutaneous adipose dataset were visualized as volcano plots by using the R package ggplot2.

Functional annotation for genes of interest

To explore DisGeNET, Gene Ontology (GO), WikiPathwas, Kyoto Encyclopedia of Genes and Genomes (KEGG) and Reactome of selected genes, Metascape was used to explore the functions among DEGs, with a cutoff criterion of $p < 0.05$. GO annotation that contains the biological process (BP) subontology, which can identify the biological properties of genes and gene sets for all organisms.

Gene set enrichment analysis (GSEA)

GSEA was performed to detect a significant difference in the set of genes expressed between the *ADGRA3* high-expressed and *ADGRA3* low-expressed groups in the enrichment of the KEGG collection.

Oxygen consumption rate (OCR)

The basal oxygen consumption rate of cells was measured using a BBoxiProbe R01 kit (BB-48211) according to the manufacturers' instructions. The maximum oxygen consumption rate of cells was measured with the addition of FCCP (Trifluoromethoxy carbonylcyanide phenylhydrazone) with a final concentration of 1μM.

Infrared Thermography.

BAT temperature was measured at room temperature by infrared thermography according to previous publications (32, 33). The same batch of representative infrared images of mice were all captured using a thermal imaging camera (FLIR ONE PRO), measured at the same distance perpendicular to the plane on which the mice were located. To quantify interscapular region temperature, the average surface temperature from a region of the interscapular BAT was taken with FLIR Tools software.

Statistical Analysis

All data are presented as mean ± *SEM*. In this study, outliers that met the three-sigma rule were excluded from analysis, with the exception of those presented in **Figure 1-figure supplement 1**E. Given the possibility that the outliers in **Figure 1-figure supplement 1**E represent extreme expressions of the inherent variability within the population sample, we have chosen to retain these specific outliers for further analysis. Student's t-test was used to compare two groups. One-way analysis of variance (ANOVA) or Two-way ANOVA was applied to compare more than two different groups on GraphPad Prism 9.0 software. For each parameter of all data presented, NS (No Significance), *$p < 0.05$, ** $p < 0.01$, *** $p < 0.001$ and **** $p < 0.0001$. $p < 0.05$ is considered significant.

Materials availability statement

Further information and requests for resources should be directed to and will be fulfilled by the lead contact, Zhonghan Yang (yangzhh@mail.sysu.edu.cn).

Data Availability

The transcriptomic dataset analyzed in this study can be accessed on the GTEx Portal database (https://gtexportal.org/home/multiGeneQueryPage), human protein atlas database (https://www.proteinatlas.org/) and GEO repository under accession number GSE118849. The PRESTO-Salsa dataset of ADGRA3 in this study can be accessed on the PRESTO-Salsa database (https://palmlab.shinyapps.io/presto-salsa/)(34). All other data generated or analyzed during this study are included in the manuscript and supporting files.

Acknowledgments

The authors are grateful for the GTEx Portal database, human protein atlas database, Gene Expression Omnibus and PRESTO-Salsa database. This research was funded by the Shenzhen Science and Technology Project (grant number: JCYJ20190807154205627), Fund of Shenzhen Key Laboratory of Systems Medicine for inflammatory diseases (grant number: ZDSYS20220606100803007) received by Zhonghan Yang. The funders had no role in study design, data collection and analysis, decision to publish, or preparation of the manuscript.

CRediT authorship contribution statement

Zewei Zhao: Investigation, Conceptualization, Data curation, Formal analysis, Writing

original draft, Writing-review & editing. **Longyun Hu:** Data curation, Formal analysis. **Bigui Song:** Data curation, Formal analysis. **Tao Jiang:** Data curation, Formal analysis. **Qian Wu:** Data curation, Formal analysis. **Jiejing Lin:** Data curation, Formal analysis. **Xiaoxiao Li:** Data curation, Formal analysis. **Yi Cai:** Data curation, Formal analysis. **Jin Li:** Data curation, Formal analysis. **Bingxiu Qian:** Data curation, Formal analysis. **Siqi Liu:** Data curation, Formal analysis. **Jilu Lang:** Conceptualization, Supervision, Writing-review & editing. **Zhonghan Yang:** Funding acquisition, Conceptualization, Supervision, Writing-review & editing.

Declaration of competing interests

The authors have declared no conflict of interest.

Abbreviations

ANOVA: analysis of variance; BAT: brown adipose tissue; β2-AR: β2-adrenoceptor; β3-AR: β3-adrenoceptor; BMI: body mass index; ADGRA3: adhesion G protein-coupled receptor A3; CL: CL-316,243; DEGs: differentially expressed genes; edgeR: Empirical Analysis of Digital Gene Expression Data in R; eWAT: epididymal white adipose tissue; FDA: Food and Drug Administration; GEO: Gene Expression Omnibus; GPCRs: G protein-coupled receptors; GSEA: Gene set enrichment analysis; NCD: normal-chow diet; HFD: high-fat diet; GTT: glucose tolerance test; HOMA-IR: homeostasis model assessment of insulin resistance; ITT: insulin tolerance test; iWAT: inguinal white adipose tissue; Limma: Linear Models for Microarray Data; Hes: Hesperetin; PKAi: protein kinase A inhibitor; NS: No Significance; RPKM: Reads Per Kilobase per Million mapped reads; TPM: Transcripts Per Kilobase Million; WT: Wild-type; GWAS: genome-wide association study; SNP: single

nucleotide polymorphism; OCR: oxygen consumption rate; SVF: Stromal Vascular Fraction; hADSCs: human adipose-derived mesenchymal stem cells; .

References

1. Organization WH. WHO Discussion Paper: Draft recommendations for the prevention and management of obesity over the life course, including potential targets 2021 [Available from: https://www.who.int/publications/m/item/who-discussion-paper-draft-recommen-dations-for-the-prevention-and-management-of-obesity-over-the-life-course-including-potential-targets.
2. Chu DT, Minh Nguyet NT, Dinh TC, Thai Lien NV, Nguyen KH, Nhu Ngoc VT, et al. An update on physical health and economic consequences of overweight and obesity. Diabetes Metab Syndr. 2018;12(6):1095-100.
3. Zhang X, Zhang M, Zhao Z, Huang Z, Deng Q, Li Y, et al. Geographic Variation in Prevalence of Adult Obesity in China: Results From the 2013-2014 National Chronic Disease and Risk Factor Surveillance. Ann Intern Med. 2019;172(4):291-3.
4. Twig G, Yaniv G, Levine H, Leiba A, Goldberger N, Derazne E, et al. Body-Mass Index in 2.3 Million Adolescents and Cardiovascular Death in Adulthood. N Engl J Med. 2016;374(25):2430-40.
5. Kim SH, Despres JP, Koh KK. Obesity and cardiovascular disease: friend or foe? Eur Heart J. 2016;37(48):3560-8.
6. Hypponen E, Mulugeta A, Zhou A, Santhanakrishnan VK. A data-driven approach for studying the role of body mass in multiple diseases: a phenome-wide registry-based case-control study in the UK Biobank. Lancet Digit Health. 2019;1(3):E116-E26.
7. Calle EE. Obesity and cancer. BMJ. 2007;335(7630):1107-8.
8. Yoneshiro T, Aita S, Matsushita M, Kayahara T, Kameya T, Kawai Y, et al. Recruited brown adipose tissue as an antiobesity agent in humans. J Clin Invest. 2013;123(8):3404-8.
9. Finlin BS, Memetimin H, Zhu B, Confides AL, Vekaria HJ, El Khouli RH, et al. The β3-adrenergic receptor agonist mirabegron improves glucose homeostasis in obese humans. J Clin Invest. 2020;130(5):2319-31.
10. Sui WH, Li HS, Yang YL, Jing X, Xue F, Cheng J, et al. Bladder drug mirabegron exacerbates atherosclerosis through activation of brown fat-mediated lipolysis. Proceedings of the National Academy of Sciences of the United States of America. 2019;116(22):10937-42.
11. Blondin DP, Nielsen S, Kuipers EN, Severinsen MC, Jensen VH, Miard S, et al. Human Brown Adipocyte Thermogenesis Is Driven by beta2-AR Stimulation. Cell Metab. 2020;32(2):287-300.e7.
12. Hauser AS, Attwood MM, Rask-Andersen M, Schioth HB, Gloriam DE. Trends in GPCR drug discovery: new agents, targets and indications. Nat Rev Drug Discov. 2017;16(12):829-42.
13. Muller TD, Bluher M, Tschop MH, DiMarchi RD. Anti-obesity drug discovery: advances and challenges. Nat Rev Drug Discov. 2021.
14. Alba M, Yee J, Frustaci ME, Samtani MN, Fleck P. Efficacy and safety of glucagon-like peptide-1/glucagon receptor co-agonist JNJ-64565111 in individuals with obesity without type 2 diabetes mellitus: A randomized dose-ranging study. Clin Obes. 2021;11(2):e12432.
15. Nybo ML, Kvam JM, Nielsen JE, Frederiksen H, Spiess K, Jensen KHR, et al. Loss of Adgra3 causes obstructive azoospermia with high penetrance in male mice. FASEB J. 2023;37(2):e22781.

16. Spiess K, Bagger SO, Torz LJ, Jensen KHR, Walser AL, Kvam JM, et al. Arrestin-independent constitutive endocytosis of GPR125/ADGRA3. Ann N Y Acad Sci. 2019;1456(1):186-99.
17. Seandel M, James D, Shmelkov SV, Falciatori I, Kim J, Chavala S, et al. Generation of functional multipotent adult stem cells from GPR125+ germline progenitors. Nature. 2007;449(7160):346-50.
18. Vizurraga A, Adhikari R, Yeung J, Yu M, Tall GG. Mechanisms of adhesion G protein-coupled receptor activation. J Biol Chem. 2020;295(41):14065-83.
19. Hamann J, Aust G, Arac D, Engel FB, Formstone C, Fredriksson R, et al. International Union of Basic and Clinical Pharmacology. XCIV. Adhesion G protein-coupled receptors. Pharmacol Rev. 2015;67(2):338-67.
20. Sakurai T, Kamakura S, Hayase J, Kohda A, Nakamura M, Sumimoto H. GPR125 (ADGRA3) is an autocleavable adhesion GPCR that traffics with Dlg1 to the basolateral membrane and regulates epithelial apicobasal polarity. J Biol Chem. 2022;298(10):102475.
21. Cha J, Choo H, Srikanth K, Lee SH, Son JW, Park MR, et al. Genome-Wide Association Study Identifies 12 Loci Associated with Body Weight at Age 8 Weeks in Korean Native Chickens. Genes (Basel). 2021;12(8).
22. Harms M, Seale P. Brown and beige fat: development, function and therapeutic potential. Nature Medicine. 2013;19(10):1252-63.
23. O'Mara AE, Johnson JW, Linderman JD, Brychta RJ, McGehee S, Fletcher LA, et al. Chronic mirabegron treatment increases human brown fat, HDL cholesterol, and insulin sensitivity. J Clin Invest. 2020;130(5):2209-19.
24. Talamonti E, Davegardh J, Kalinovich A, van Beek SMM, Dehvari N, Halleskog C, et al. The novel adrenergic agonist ATR-127 targets skeletal muscle and brown adipose tissue to tackle diabesity and steatohepatitis. Mol Metab. 2024;85:101931.
25. Fisher FM, Kleiner S, Douris N, Fox EC, Mepani RJ, Verdeguer F, et al. FGF21 regulates PGC-1alpha and browning of white adipose tissues in adaptive thermogenesis. Genes Dev. 2012;26(3):271-81.
26. Kajimura S, Spiegelman BM, Seale P. Brown and Beige Fat: Physiological Roles beyond Heat Generation. Cell Metabolism. 2015;22(4):546-59.
27. Hizawa N. Pharmacogenetics of β2-agonists. Allergol Int. 2011;60(3):239-46.
28. Morell A, Milara J, Gozalbes L, Gavaldà A, Tarrasón G, Godessart N, et al. β2-adrenoreceptors control human skin microvascular reactivity. Eur J Dermatol. 2021;31(3):326-34.
29. Yeh CH, Shen ZQ, Wang TW, Kao CH, Teng YC, Yeh TK, et al. Hesperetin promotes longevity and delays aging via activation of Cisd2 in naturally aged mice. J Biomed Sci. 2022;29(1):53.
30. Xue M, Weickert MO, Qureshi S, Kandala NB, Anwar A, Waldron M, et al. Improved Glycemic Control and Vascular Function in Overweight and Obese Subjects by Glyoxalase 1 Inducer Formulation. Diabetes. 2016;65(8):2282-94.
31. Subash-Babu P, Alshatwi AA. Hesperetin inhibit adipocyte differentiation and enhance Bax- and p21-mediated adipolysis in human mesenchymal stem cell adipogenesis. J Biochem Mol Toxicol. 2015;29(3):99-108.
32. Xia B, Shi XC, Xie BC, Zhu MQ, Chen Y, Chu XY, et al. Urolithin A exerts antiobesity effects through enhancing adipose tissue thermogenesis in mice. PLoS Biol. 2020;18(3):e3000688.
33. Warner A, Rahman A, Solsjö P, Gottschling K, Davis B, Vennström B, et al. Inappropriate heat dissipation ignites brown fat thermogenesis in mice with a mutant thyroid hormone receptor α1. Proc Natl Acad Sci U S A. 2013;110(40):16241-6.
34. Chen H, Rosen CE, Gonzalez-Hernandez JA, Song D, Potempa J, Ring AM, et al. Highly multiplexed bioactivity screening reveals human and microbiota metabolome-GPCRome interactions. Cell. 2023;186(14):3095-110 e19.

Legends of figures and supplementary files

Figure 1. ADGRA3 is a high-expressed GPCR in human adipocytes and mouse brown fat. (A-F) ADGRA3 screening as a high-expressed GPCR in human adipocytes and mouse brown fat via comprehensive analysis. Brown adipose tissue and subcutaneous WAT were dissected from mice that were treated in cold (4°C) temperature for 72 hours. A total of six samples with three replicates for each adipose tissue were evaluated. The datasets of human subcutaneous adipocytes and human visceral adipocytes were acquired from the human protein atlas database. (A) Flowchart of screening. (B) Volcano plot summarizing the differentially expressed genes (DEGs) between cold temperature BAT group and cold temperature iWAT group. Blue and red shading are used to indicate down-regulation and up-regulation, respectively. (C) 27 BAT-elevated GPCRs from transcriptome, 515 very high genes in subcutaneous adipocytes and 462 very high genes in visceral adipocytes from the human protein atlas database were analyzed by using a Venn diagram. (D-E) The RPKM of *ADRB3* and *ADGRA3* genes in mouse fat (D) from Mouse ENCODE transcriptome data (PRJNA66167, N = 2) and human fat (E) from HPA RNA-seq normal tissues (PRJEB4337, N = 3). (F) C57BL/6J mice fed with a NCD or a HFD for 12 weeks. Representative images of iWAT and BAT stained with ADGRA3. Scale bars, 250μm. (G) C57BL/6J mice fed with a HFD for 12 weeks were injected with vehicle or CL (1 mg/kg daily) over 7 days. Representative images of iWAT and BAT stained with ADGRA3. Scale bars, 250μm. (H) Correlation between *UCP1* expression level normalized by *ACTB* gene and *ADGRA3* expression level normalized by *ACTB* gene in human subcutaneous fat dataset from GTEx

Portal database (N = 663). (I) qPCR analysis of *Adgra3*, *Adipoq* and *Ucp1* genes in Stromal Vascular Fraction (SVF) and mature adipocyte isolated from iWAT and BAT (N = 3 for each group). iWAT, inguinal white adipose tissue; BAT, brown adipose tissue; RPKM, Reads Per Kilobase per Million mapped reads; TPM, Transcripts Per Kilobase Million; GPCR, G-protein-coupled receptor; NCD, normal chow diet; HFD, high-fat diet; CL, CL-316,243; SVF, Stromal Vascular Fraction. All data are presented as mean ± *SEM*. Statistical significance was determined by unpaired two-tailed student's t-test (D-E), simple linear regression (H) and one-way ANOVA (I).

Figure 2. *Adgra3* overexpression promotes the biogenesis of beige adipocytes. (A, H) qPCR analysis of *Adgra3*, thermogenesis and lipolysis genes in 3T3-L1 mature beige-like adipocytes (A: N = 3 for each group; H: N = 4 for CON, N = 5 for *Adgra3* OE). (B, I) Western blot analysis for level of ADGRA3, UCP1 and ADGRA3-3×FLAG protein in 3T3-L1 mature beige-like adipocytes treated with sh*Adgra3* (pLKO.1-U6-sh*Adgra3*-(1/2/3) plasmid encapsulated in nanomaterials), shNC (pLKO.1-U6-shNC plasmid encapsulated in nanomaterials), *Adgra3* OE (pLV3-CMV-*Adgra3*(mouse)-3×FLAG plasmid encapsulated in nanomaterials) or CON (pLV3-CMV-MCS-3×FLAG plasmid encapsulated in nanomaterials). The ImageJ software was used for gray scanning. (C, J) Bodipy green staining for lipid droplet and Mito-Tracker red staining for mitochondria in 3T3-L1 mature beige-like adipocytes. Scale bars, 200 μm. (D, K) The level of intracellular triglyceride in 3T3-L1 mature beige-like adipocytes (D: N = 3 for each group; K: N = 4 for each group). (E, I)

Glucose uptake assay in 3T3-L1 mature beige-like adipocytes and staining intensity analysis diagram (right, N = 4 for each group). (F, M) When 3T3-L1 mature beige-like adipocytes were treated with shNC, sh*Adgra3*, CON or *Adgra3* OE, fluorescence of the oxygen probe (RO1) in the cells was monitored and the rate of basal oxygen consumption was analyzed (N = 4 for each group). (G, N) When FCCP-treaded 3T3-L1 mature beige-like adipocytes were treated with shNC, sh*Adgra3*, CON or *Adgra3* OE, fluorescence of the oxygen probe (RO1) in the cells was monitored and the rate of maximum oxygen consumption was analyzed (G: N = 6 for each group; N: N = 5 for each group). All data are presented as mean ± *SEM*. Statistical significance was determined by unpaired two-tailed student's t-test (E-H and K-N) and one-way ANOVA (A and D).

Figure 3. Knockdown of *Adgra3* suppressed the adipose thermogenic program and impaired metabolic homeostasis in mice. (A) Experimental schematic. C57BL/6J mice fed with a NCD for eight weeks were injected with sh*Adgra3* (pLKO.1-U6-sh*Adgra3*-2 plasmid encapsulated in nanomaterials) or shNC (pLKO.1-U6-shNC plasmid encapsulated in nanomaterials) twice a week for four weeks. (B-D) Changes in body mass (B), tissue weight (C) and body temperature (D) in mice injected with shNC or sh*Adgra3* for 28 days (N = 5 for each group). (E) Thermal image and BAT temperature of mice injected with shNC or sh*Adgra3* for 28 days (N = 5 for each group). (F-G) qPCR analysis of *Adgra3*, genes associated with thermogenesis and lipolysis in iWAT (F) and BAT (G) from different treatment mice (N = 5 for each group). (H-I) Western-blot analysis for the level of ADGRA3

and UCP1 protein in iWAT (H) and BAT (I) from differently treated mice. (J) Representative images of iWAT (top) and BAT (bottom) stained with UCP1. Scale bars, 250 μm. (K) Transmission electron microscope photograph of BAT treated with shNC or sh*Adgra3*. (L) Glucose tolerance test (GTT) was conducted by intraperitoneal injection of glucose (2g/kg) and measurement of blood glucose concentration with a OneTouch Ultra Glucometer at designed time points in six hours fasted mice (N = 5 for each group). (M) Insulin tolerance test (ITT) was done by intraperitoneal injection of insulin (0.5U/kg) and measurement of blood glucose concentration by a OneTouch Ultra Glucometer at designed time points in six hours fasted mice (N = 5 for each group). (N-O) The fasting serum insulin (N) and HOMA-IR (O) in mice injected with either shNC or sh*Adgra3* for 28 days (N = 5 for each group). HOMA-IR=Fasting glucose level (mmol/L) * Fasting insulin level (mIU/L) /22.5. NCD, normal chow diet; iWAT, inguinal white adipose tissue; BAT, brown adipose tissue; GTT, Glucose tolerance test; ITT, Insulin tolerance test; HOMA-IR, homeostasis model assessment of insulin resistance. All data are presented as mean ± *SEM*. Statistical significance was determined by unpaired two-tailed student's t-test (C-G and N-O) and two-way ANOVA (B and L-M).

Figure 4. *Adgra3* overexpression activated the adipose thermogenic program and facilitated metabolic homeostasis in mice with diet-induced obesity (DIO). (A) Experimental schematic. C57BL/6J mice were fed with a HFD and injected with *Adgra3* OE (pLV3-CMV-*Adgra3* (mouse)-3×FLAG plasmid encapsulated in nanomaterials) or CON

(pLV3-CMV-MCS-3×FLAG plasmid encapsulated in nanomaterials) once a week for 12 weeks. (B-D) Changes in body mass (B), tissue weight (C) and body temperature (D) of mice injected with CON or *Adgra3* OE (N = 6 for each group). (E) Thermal image and BAT temperature in mice injected with CON or *Adgra3* OE (N = 6 for each group). (F-G) qPCR analysis of *Adgra3*, genes associated with thermogenesis and lipolysis in iWAT (F) and BAT (G) from different treatment mice (N = 3 for each group). (H-I) Western-blot analysis for the level of ADGRA3-3×FLAG and UCP1 protein in iWAT (H) and BAT (I) from differently treated mice. (J) Representative images of iWAT (top; Scale bars, 50 μm.) and BAT (bottom; Scale bars, 50 μm.) stained with UCP1. (K) Transmission electron microscope photograph of BAT treated with CON or *Adgra3* OE. (L) Glucose tolerance test (GTT) was conducted by intraperitoneal injection of glucose (1g/kg) and measurement of blood glucose concentration with a OneTouch Ultra Glucometer at designed time points in six hours fasted mice (N = 6 for each group). (M) Insulin tolerance test (ITT) was done by intraperitoneal injection of insulin (1U/kg) and measurement of blood glucose concentration by a OneTouch Ultra Glucometer at designed time points in six hours fasted mice (N = 6 for each group). (N-O) The fasting serum insulin (N) and HOMA-IR (O) in mice injected with CON or *Adgra3* OE (N = 6 for each group). HOMA-IR=Fasting glucose level (mmol/L) * Fasting insulin level (mIU/L) /22.5. HFD, high-fat diet; iWAT, inguinal white adipose tissue; BAT, brown adipose tissue; GTT, Glucose tolerance test; ITT, Insulin tolerance test; HOMA-IR, homeostasis model assessment of insulin resistance. All data are presented as mean ± *SEM*. Statistical significance was determined by unpaired two-tailed student's t-test (C-G and N-O) and two-way ANOVA (B and L-M).

Figure 5. ADGRA3 promotes the biogenesis of beige adipocytes via the Gs-PKA-CREB axis. (A-B) Western-blot analysis for level of ADGRA3-3×FLAG, GNAS-6×HIS and HSP90 proteins in 293T transfected with different plasmids. (C-D) The level of cAMP in 3T3-L1. An ELISA kit was used to measure the level of cAMP (N = 6 for each group). (E, G and I-J) Western-blot analysis for level of ADGRA3, ADGRA3-3×FLAG, UCP1, p-CREB and CREB protein in 3T3-L1 mature beige-like adipocytes. (F and H) Western-blot analysis for level of p-CREB and CREB proteins in iWAT and BAT from differently treated mice. PKAi, protein kinase A inhibitor, 20 μM H-89. All data are presented as mean ± *SEM*. Statistical significance was determined by unpaired two-tailed student's t-test (C) and one-way ANOVA (D).

Figure 6. Hesperetin promotes the biogenesis of beige adipocytes via ADGRA3-G_s-PKA-CREB axis. (A) Table of human metabolites with the ability to activate ADGRA3, from the PRESTO-Salsa database. (B) The level of cAMP in 3T3-L1. ELISA kit was used to measure the level of cAMP (N = 3 for each group). (C, E, I and K) qPCR analysis of *Adgra3*, *Gnas* and *Ucp1* in 3T3-L1 mature beige-like adipocytes (N = 3 for each group). (D, F, J and L) Western-blot analysis for level of ADGRA3, GNAS, UCP1, p-CREB and CREB protein in 3T3-L1 mature beige-like adipocytes. (G) When 3T3-L1 mature beige-like adipocytes were treated with shNC, sh*Adgra3*, or Hesperetin, fluorescence of the oxygen probe (RO1) in the

cells was monitored and the rate of basal oxygen consumption was analyzed (N = 5 for sh*Adgra3*-Veh; N = 6 for each other group). (H) When FCCP-treaded 3T3-L1 mature beige-like adipocytes were treated with shNC, sh*Adgra3*, or Hesperetin, fluorescence of the oxygen probe (RO1) in the cells was monitored and the rate of maximum oxygen consumption was analyzed (N = 4 for shNC-Veh; N = 3 for each other group). Hes, 10 μM Hesperetin; PKAi, protein kinase A inhibitor, 20 μM H-89. All data are presented as mean ± *SEM*. Statistical significance was determined by unpaired two-tailed student's t-test (B-C) and one-way ANOVA (E, G-I and K).

Figure 7. Hesperetin activated the adipose thermogenic program and facilitated metabolic homeostasis in mice with diet-induced obesity (DIO) dependent on ADGRA3. (A) Experimental schematic. Different treated C57BL/6J mice were fed with a HFD for 12 weeks. (B-D) Changes in body mass (B), tissue weight (C) and body temperature (D) of different treated mice (N = 6 for HFD-shNC and HFD-sh*Adgra3*; N = 5 for HFD-shNC-Hes and HFD-sh*Adgra3*-Hes). (E) Thermal image and BAT temperature of different treated mice (N = 6 for HFD-shNC and HFD-sh*Adgra3*; N = 5 for HFD-shNC-Hes and HFD-sh*Adgra3*-Hes). (F-G) qPCR analysis of *Adgra3* and *Ucp1* in iWAT (F) and BAT (G) from different treated mice (N = 3 for each group). (H-I) Representative images of iWAT (H; Scale bars, 50 μm.) and BAT (I; Scale bars, 50 μm.) stained with UCP1. (J) Transmission electron microscope photograph of BAT from different treated mice (Scale bars, 2 μm.). (K) Glucose tolerance test (GTT) was conducted by intraperitoneal injection of glucose (1g/kg) and measurement of blood glucose concentration with a OneTouch Ultra Glucometer at designed

time points in six hours fasted mice (N = 6 for HFD-shNC and HFD-sh*Adgra3*; N = 5 for HFD-shNC-Hes and HFD-sh*Adgra3*-Hes). (L) Insulin tolerance test (ITT) was done by intraperitoneal injection of insulin (1U/kg) and measurement of blood glucose concentration by a OneTouch Ultra Glucometer at designed time points in six hours fasted mice (N = 6 for HFD-shNC and HFD-sh*Adgra3*; N = 5 for HFD-shNC-Hes and HFD-sh*Adgra3*-Hes). (M-N) The fasting serum insulin (M) and HOMA-IR (N) in different treated mice (N = 6 for HFD-shNC and HFD-sh*Adgra3*; N = 5 for HFD-shNC-Hes and HFD-sh*Adgra3*-Hes). HOMA-IR=Fasting glucose level (mmol/L) * Fasting insulin level (mIU/L) /22.5. HFD, high-fat diet; iWAT, inguinal white adipose tissue; BAT, brown adipose tissue; GTT, Glucose tolerance test; ITT, Insulin tolerance test; HOMA-IR, homeostasis model assessment of insulin resistance; Hes, Hesperetin. All data are presented as mean ± *SEM*. Statistical significance was determined by one-way ANOVA (C-G and M-N) and two-way ANOVA (B and K-L).

Figure 8. *ADGRA3* overexpression induces the beiging of human adipocytes. (A-B) qPCR analysis of *ADGRA3* and *UCP1* genes in adipocytes induced from human adipose-derived mesenchymal stem cells (hADSCs) (A: N = 3 for each group; B: N = 4 for each group). (C-D) Bodipy green staining for lipid droplet and Mito-Tracker red staining for mitochondria in adipocytes induced from hADSCs. Scale bars, 150 μm. (E-H) qPCR analysis of *Adgra3* and *Ucp1* genes in mouse primary adipocytes induced from stromal vascular fraction (SVF) of WAT (E-H: N = 3 for each group). sh*ADGRA3* (pLKO.1-U6-sh*ADGRA3*-(1/2/3) plasmid encapsulated in nanomaterials), shNC (pLKO.1-U6-shNC plasmid encapsulated in

nanomaterials), *ADGRA3* OE (pLV3-CMV-*ADGRA3*(human)-3×FLAG plasmid encapsulated in nanomaterials) or CON (pLV3-CMV-MCS-3×FLAG plasmid encapsulated in nanomaterials). All data are presented as mean ± *SEM*. Statistical significance was determined by unpaired two-tailed student's t-test (B and E-F) and one-way ANOVA (A and G-H).

Figure 9. Graphical abstract. This schema summarizes the main roles and functions of ADGRA3 in lipid metabolism. ADGRA3 promotes the biogenesis of beige adipocytes via the Gs-PKA-CREB axis. This figure was drawn by Figdraw (Copyright ID: IWAIA0d9f9).

Supplementary File 1. Primer sequences used for qPCR.

Supplementary File 2. Gene annotation for screened genes. The 1134 screened genes were annotated by David database and 27 of these genes were identified as G-protein coupled receptor encoding gene.

Figure 1-figure supplement 1. ADGRA3 positively correlated with beige fat. (A-B) qPCR analysis of *Adgra3* and *Ucp1* in iWAT and BAT from different treatment mice (A: N = 3 for each group; B: N = 4 for iWAT-CON, N = 5 for each other group). (C) C57BL/6J mice fed with a NCD or a HFD for 12 weeks. Representative images of iWAT and BAT stained with

UCP1. Scale bars, 250μm. (D) C57BL/6J mice fed with a HFD for 12 weeks were injected with vehicle or CL (1 mg/kg daily) over 7 days. Representative images of iWAT and BAT stained with UCP1. Scale bars, 250μm. (E) The TPM of *ADRB2*, *ADRB3* and *ADGRA3* genes in human scWAT (left, N = 663) and viWAT (right, N = 541) from the GTEx database. (F) Correlation between *UCP1* expression level normalized by *ACTB* gene and *ADRB3* expression level normalized by *ACTB* gene in human subcutaneous fat dataset from GTEx Portal database (N = 663). (G) qPCR analysis of *Adgra3* and *Ucp1* during the differentiation of 3T3-L1 into adipocytes (N = 3 for each group). (H) qPCR analysis of *ADGRA3* and *UCP1* during the differentiation of hADSCs into adipocytes (N = 3 for each group). iWAT, inguinal white adipose tissue; BAT, brown adipose tissue; scWAT, subcutaneous white adipose tissue; viWAT, visceral white adipose tissue; NCD, normal chow diet; HFD, high-fat diet; CL: CL-316,243; qPCR, quantitative real-time PCR; hADSCs, human adipose-derived mesenchymal stem cells. All data are presented as mean ± *SEM*. Statistical significance was determined by one-way ANOVA (A-B, E and G-H) and simple linear regression (F).

Figure 3-figure supplement 1. Characterization of wild-type and *Adgra3*-knockdown mice. (A-H) C57BL/6J mice fed with a NCD for eight weeks were injected with sh*Adgra3* (pLKO.1-U6-sh*Adgra3*-2 plasmid encapsulated in nanomaterials) or shNC (pLKO.1-U6-shNC plasmid encapsulated in nanomaterials) twice a week for four weeks. (A) qPCR analysis of *Adgra3* gene in iWAT, BAT, heart, liver and spleen from different treatment mice (N = 4 for each group). (B) qPCR analysis of *Adgra3* gene in lung, kidney, stomach, skeletal muscle and brain from different treatment mice (N = 4 for each group). (C) Food intake of

different treated mice (N = 4 for each group). (D-E) The TG level of serum (D) and liver (E) from different treated mice (N = 5 for each group). (F) Representative images of iWAT (top) and BAT (bottom) stained with hematoxylin and eosin. Scale bars, 250 μm. (G) Representative images of eWAT (top) and Liver (bottom) stained with hematoxylin and eosin. Scale bars, 250 μm. (H) The fT4 level of serum from different treated mice (N = 5 for each group). (I) Schematic depicting the site-directed nanomaterials-encapsulated nucleic acid injections used to knockdown *Adgra3* in BAT. (J) qPCR analysis of *Adgra3*, genes associated with thermogenesis and lipolysis in different-treated BAT (N = 4 for each group). shNC, pLKO.1-U6-shNC plasmid encapsulated in nanomaterials; sh*Adgra3*, pLKO.1-U6-sh*Adgra3*-2 plasmid encapsulated in nanomaterials; iWAT, inguinal white adipose tissue; eWAT, epididymal white adipose tissue; BAT, brown adipose tissue; NCD, normal chow diet; fT4, free tetraiodothyronine. All data are presented as mean ± *SEM*. Statistical significance was determined by paired two-tailed student's t-test (C) and unpaired two-tailed student's t-test (A-B, D-E, H and J).

Figure 3-figure supplement 2. *ADGRA3* high expressed gene sets in human subcutaneous fat are enriched to lipid metabolism and adipocyte differentiation. (A) Volcano plot summarizing the differentially expressed genes (DEGs) between *ADGRA3* high-expressed human subcutaneous adipose group and *ADGRA3* low-expressed human subcutaneous adipose group. Blue and red shading indicates down-regulation and up-regulation, respectively. (B-F) Enrichment analysis for the high-expressed genes in *ADGRA3* high-expressed human subcutaneous adipose in DisGeNET (B), GO-Biological Process (C),

WikiPathways (D), KEGG (E) and Reactome (F) databases. (G-H) Gene set enrichment analysis (GSEA) analysis for gene signatures of insulin signaling pathway in human subcutaneous adipose (G) and human visceral adipose (H) from *ADGRA3* high-expressed group compared with *ADGRA3* low-expressed group. NES, normalized enrichment score. FDR, false discovery rate.

Figure 4-figure supplement 1. *Adgra3* overexpression activated the adipose thermogenic program in mice. (A) Experimental schematic. C57BL/6J mice fed with a NCD for eight weeks were injected with *Adgra3* OE (pLV3-CMV-*Adgra3*(mouse)-3×FLAG plasmid encapsulated in nanomaterials) or CON (pLV3-CMV-MCS-3×FLAG plasmid encapsulated in nanomaterials) twice a week for four weeks. (B) qPCR analysis of *Adgra3* gene in iWAT, BAT, heart, liver and spleen from different treatment mice (N = 4 for each group). (C) qPCR analysis of *Adgra3* gene in lung, kidney, stomach, skeletal muscle and brain from different treatment mice (N = 4 for each group). (D) Body temperature of mice injected with CON or *Adgra3* OE for 28 days (N = 5 for each group). (E) Thermal image and BAT temperature in mice injected with CON or *Adgra3* OE for 28 days (N = 5 for each group). (F) The fT4 level of serum from different treated mice (N = 5 for each group). (G) Representative images of iWAT (top) and BAT (bottom) stained with HE. Scale bars, 100 μm. (H-I) qPCR analysis of *Adgra3*, genes associated with thermogenesis and lipolysis in iWAT (H) and BAT (I) from different treatment mice (N = 3 for each group). (J-K) Western-blot analysis for the level of ADGRA3-3×FLAG and UCP1 protein in iWAT (J) and BAT (K) from differently treated mice. The ImageJ software was used for gray scanning. (L) Representative images of iWAT

(top; Scale bars, 100 μm.) and BAT (bottom; Scale bars, 250 μm.) stained with UCP1. NCD, normal chow diet; iWAT, inguinal white adipose tissue; BAT, brown adipose tissue; fT4, free tetraiodothyronine. All data are presented as mean ± *SEM*. Statistical significance was determined by unpaired two-tailed student's t-test (B-F and H-I).

Figure 4-figure supplement 2. Characterization of wild-type and *Adgra3*-overexpressed mice. (A-F) C57BL/6J mice were fed with a HFD and injected with *Adgra3* OE (pLV3-CMV-Adgra3 (mouse)-3×FLAG plasmid encapsulated in nanomaterials) or CON (pLV3-CMV-MCS-3×FLAG plasmid encapsulated in nanomaterials) once a week for 12 weeks. (A) Food intake of different treated mice (N = 6 for each group). (B) The fT4 level of serum from different treated mice (N = 6 for each group). (C-D) The TG level of serum (C) and liver (D) from different treated mice (N = 6 for each group). (E) Representative images of iWAT (top) and BAT (bottom) stained with hematoxylin and eosin. Scale bars, 50 μm. (F) Representative images of eWAT (top) and Liver (bottom) stained with hematoxylin and eosin. Scale bars, 50 μm. (G) Schematic depicting the site-directed nanomaterials-encapsulated nucleic acid injections used to overexpress *Adgra3* in BAT. (H) qPCR analysis of *Adgra3*, genes associated with thermogenesis and lipolysis in different-treated BAT (N = 4 for each group). HFD, high-fat diet; iWAT, inguinal white adipose tissue; BAT, brown adipose tissue; fT4, free tetraiodothyronine. All data are presented as mean ± SEM. Statistical significance was determined by paired two-tailed student's t-test (A) and unpaired two-tailed student's t-test (B-D and H).

Figure 5-figure supplement 1. ADGRA3 was not observed to bind to G_i, G_q and G_{12}. (A-C) Western-blot analysis for level of ADGRA3-3×FLAG, GNAI1-6×HIS (A), GNAQ-6×HIS (B), GNA12-6×HIS (C) and HSP90 proteins in 293T transfected with different plasmids. (D) The level of IP1 in 3T3-L1 (N = 6 for each group). An ELISA kits was used to measure the level of IP1. (E-F) qPCR analysis of *Gnas*, *Adgra3* and *Ucp1* in 3T3-L1 mature beige-like adipocytes (N = 3 for each group). PKAi, protein kinase A inhibitor, 20 μM H-89. All data are presented as mean ± *SEM*. Statistical significance was determined by unpaired two-tailed student's t-test (D) and one-way ANOVA (E-F).

Figure 7-figure supplement 1. Characterization of wild-type and *Adgra3*-knockdown mice after hesperetin treatment. (A) Food intake of different treated mice (N = 5 for each group). (B) The fT4 level of serum from different treated mice (N = 6 for HFD-shNC and HFD-sh*Adgra3*; N = 5 for HFD-shNC-Hes and HFD-sh*Adgra3*-Hes). (C-D) The TG level of serum (C) and liver (D) from different treated mice (N = 6 for HFD-shNC and HFD-sh*Adgra3*; N = 5 for HFD-shNC-Hes and HFD-sh*Adgra3*-Hes). (E-F) Representative images of iWAT (E) and BAT (F) stained with hematoxylin and eosin. Scale bars, 50 μm. HFD, high-fat diet; iWAT, inguinal white adipose tissue; BAT, brown adipose tissue; fT4, free tetraiodothyronine, Hes, Hesperetin. All data are presented as mean ± *SEM*. Statistical significance was determined by one-way ANOVA (A-D).

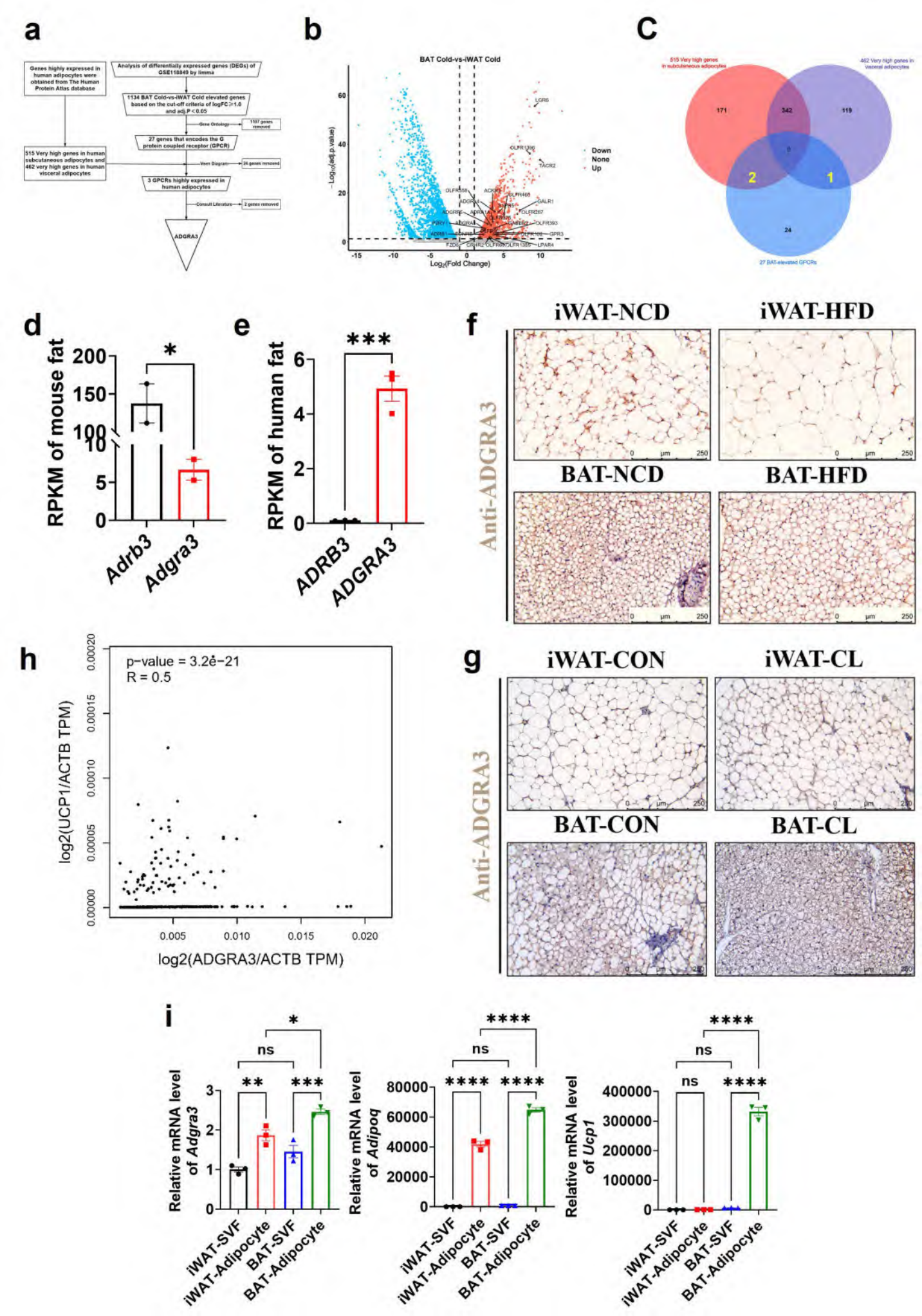
a
Genes highly expressed in human adipocytes were obtained from The Human Protein Atlas database
Analysis of differentially expressed genes (DEGs) of GSE118849 by limma
1134 BAT Cold-vs-iWAT Cold elevated genes based on the cut-off criteria of logFC≥1.0 and adj.P<0.05
Gene Ontology
1107 genes removed
27 genes that encodes the G protein coupled receptor (GPCR)
515 Very high genes in human subcutaneous adipocytes and 462 very high genes in human visceral adipocytes
Venn Diagram
24 genes removed
3 GPCRs highly expressed in human adipocytes
Consult Literature
2 genes removed
ADGRA3
b
BAT Cold-vs-iWAT Cold
Down
None
Up
Log2(Fold Change)
−Log10(adj.p.value)
c
515 Very high genes in subcutaneous adipocytes
462 Very high genes in visceral adipocytes
27 BAT-elevated GPCRs
171
342
119
0
2
1
24
d
RPKM of mouse fat
Adrb3
Adgra3
e
RPKM of human fat
ADRB3
ADGRA3
f
iWAT-NCD
iWAT-HFD
BAT-NCD
BAT-HFD
Anti-ADGRA3
g
iWAT-CON
iWAT-CL
BAT-CON
BAT-CL
Anti-ADGRA3
h
p−value = 3.2e−21
R = 0.5
log2(UCP1/ACTB TPM)
log2(ADGRA3/ACTB TPM)
i
Relative mRNA level of Adgra3
Relative mRNA level of Adipoq
Relative mRNA level of Ucp1
iWAT-SVF
iWAT-Adipocyte
BAT-SVF
BAT-Adipocyte

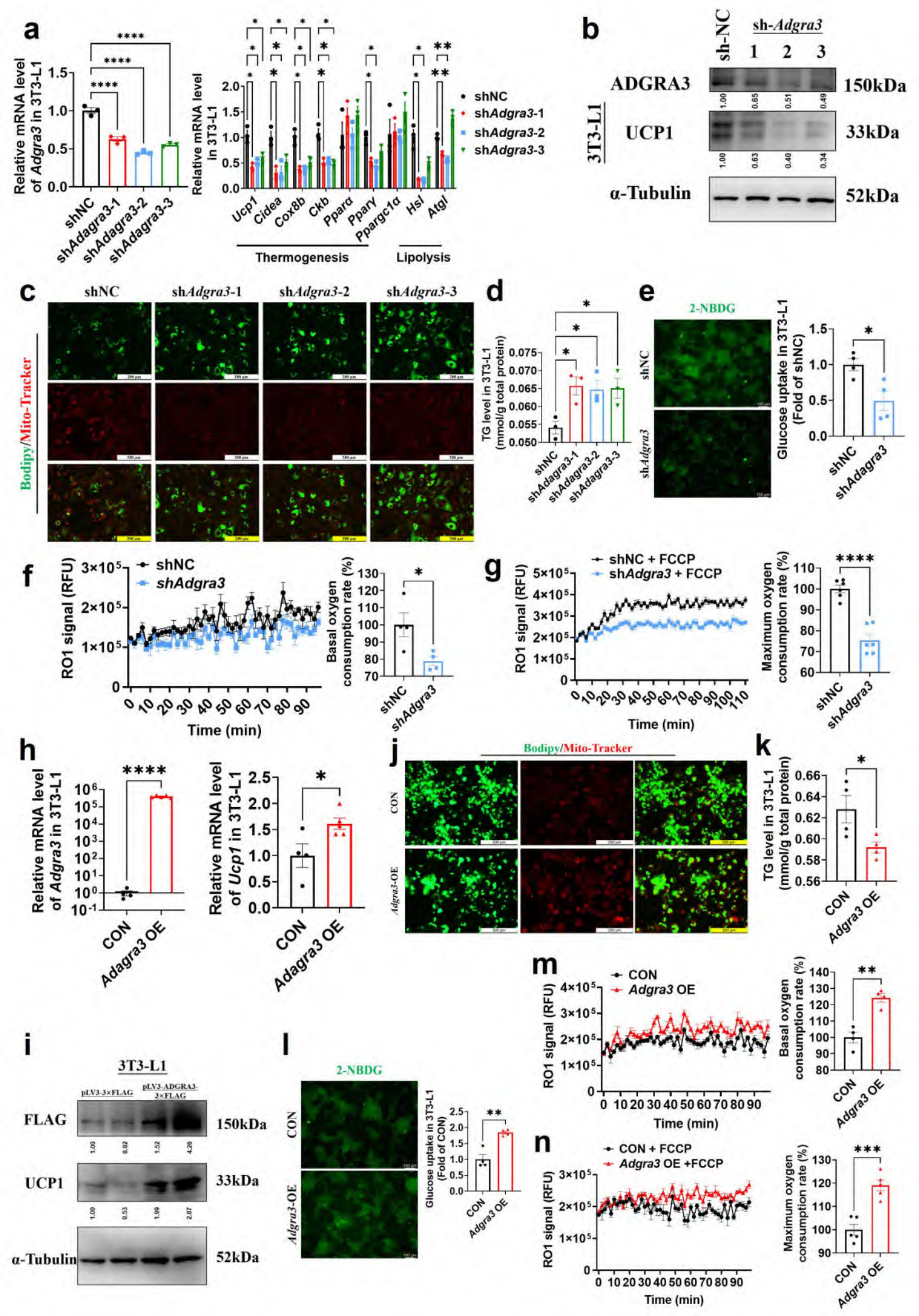
a
Relative mRNA level of Adgra3 in 3T3-L1
shNC
shAdagra3-1
shAdagra3-2
shAdagra3-3
Relative mRNA level in 3T3-L1
shNC
shAdgra3-1
shAdgra3-2
shAdgra3-3
Ucp1
Cidea
Cox8b
Ckb
Pparα
Pparγ
Ppargc1α
Hsl
Atgl
Thermogenesis
Lipolysis
b
sh-NC
sh-Adgra3
1
2
3
ADGRA3
150kDa
1.00
0.65
0.51
0.49
3T3-L1
UCP1
33kDa
1.00
0.63
0.40
0.34
α-Tubulin
52kDa
c
shNC
shAdgra3-1
shAdgra3-2
shAdgra3-3
Bodipy/Mito-Tracker
d
TG level in 3T3-L1 (mmol/g total protein)
shNC
shAdagra3-1
shAdagra3-2
shAdagra3-3
e
2-NBDG
shNC
shAdgra3
Glucose uptake in 3T3-L1 (Fold of shNC)
shNC
shAdagra3
f
RO1 signal (RFU)
shNC
shAdgra3
Time (min)
Basal oxygen consumption rate (%)
shNC
shAdgra3
g
shNC + FCCP
shAdgra3 + FCCP
RO1 signal (RFU)
Time (min)
Maximum oxygen consumption rate (%)
shNC
shAdgra3
h
Relative mRNA level of Adgra3 in 3T3-L1
CON
Adagra3 OE
Relative mRNA level of Ucp1 in 3T3-L1
CON
Adagra3 OE
j
Bodipy/Mito-Tracker
CON
Adgra3-OE
k
TG level in 3T3-L1 (mmol/g total protein)
CON
Adagra3 OE
i
3T3-L1
pLV3-3×FLAG
pLV3-ADGRA3-3×FLAG
FLAG
150kDa
1.00
0.92
1.52
4.26
UCP1
33kDa
1.00
0.53
1.99
2.87
α-Tubulin
52kDa
l
2-NBDG
CON
Adgra3-OE
Glucose uptake in 3T3-L1 (Fold of CON)
CON
Adgra3 OE
m
CON
Adgra3 OE
RO1 signal (RFU)
Time (min)
Basal oxygen consumption rate (%)
CON
Adgra3 OE
n
CON + FCCP
Adgra3 OE +FCCP
RO1 signal (RFU)
Time (min)
Maximum oxygen consumption rate (%)
CON
Adgra3 OE

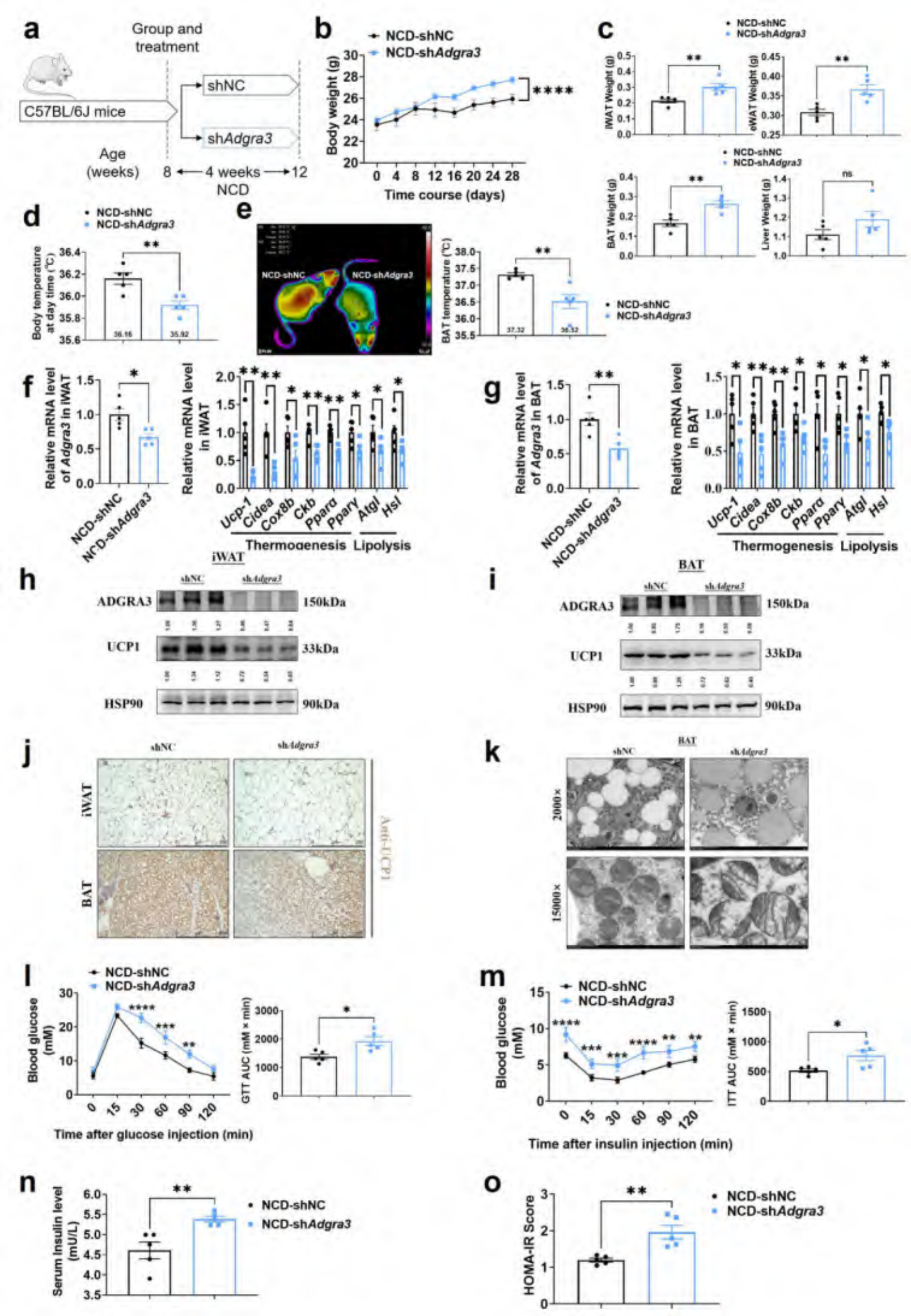
a
Group and treatment
C57BL/6J mice
shNC
shAdgra3
Age (weeks)
8
4 weeks NCD
12
b
NCD-shNC
NCD-shAdgra3
Body weight (g)
Time course (days)
c
iWAT Weight (g)
eWAT Weight (g)
BAT Weight (g)
Liver Weight (g)
d
Body temperature at day time (℃)
e
NCD-shNC
NCD-shAdgra3
BAT temperature (℃)
f
Relative mRNA level of Adgra3 in iWAT
Relative mRNA level in iWAT
Ucp-1
Cidea
Cox8b
Ckb
Pparα
Pparγ
Atgl
Hsl
Thermogenesis
Lipolysis
g
Relative mRNA level of Adgra3 in BAT
Relative mRNA level in BAT
h
iWAT
shNC
shAdgra3
ADGRA3
150kDa
UCP1
33kDa
HSP90
90kDa
i
BAT
j
iWAT
BAT
Anti-UCP1
k
2000×
15000×
l
Blood glucose (mM)
Time after glucose injection (min)
GTT AUC (mM × min)
m
Time after insulin injection (min)
ITT AUC (mM × min)
n
Serum Insulin level (mU/L)
o
HOMA-IR Score

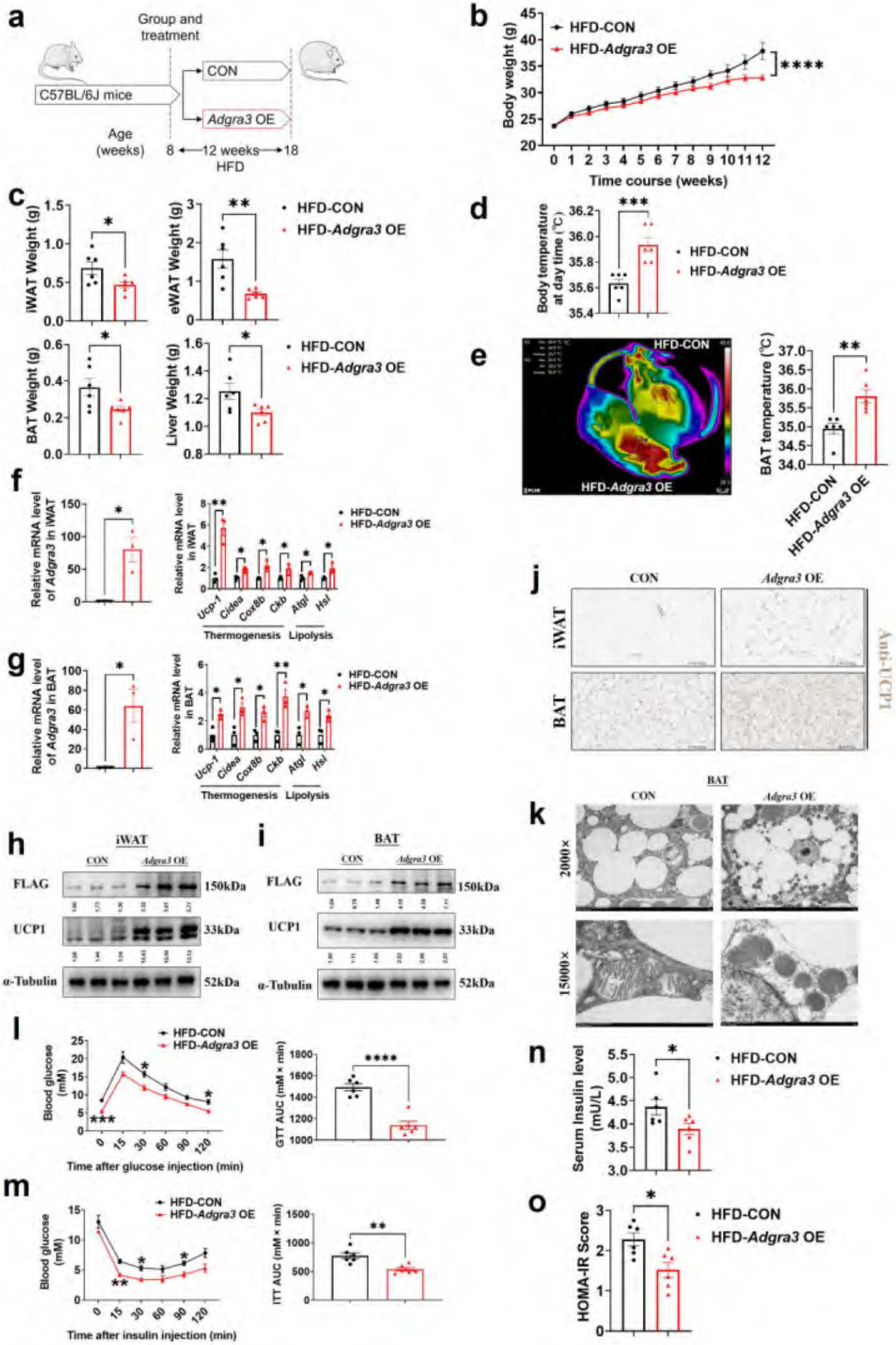
a
Group and treatment
C57BL/6J mice
CON
Adgra3 OE
Age (weeks)
8 ← 12 weeks → 18
HFD
b
HFD-CON
HFD-Adgra3 OE
Body weight (g)
Time course (weeks)
****
c
iWAT Weight (g)
eWAT Weight (g)
BAT Weight (g)
Liver Weight (g)
HFD-CON
HFD-Adgra3 OE
d
Body temperature at day time (℃)
***
e
HFD-CON
HFD-Adgra3 OE
BAT temperature (℃)
**
f
Relative mRNA level of Adgra3 in iWAT
Relative mRNA level in iWAT
Ucp-1
Cidea
Cox8b
Ckb
Atgl
Hsl
Thermogenesis
Lipolysis
g
Relative mRNA level of Adgra3 in BAT
Relative mRNA level in BAT
h
iWAT
CON
Adgra3 OE
FLAG
150kDa
UCP1
33kDa
α-Tubulin
52kDa
i
BAT
j
iWAT
BAT
Anti-UCP1
k
2000×
15000×
l
Blood glucose (mM)
Time after glucose injection (min)
GTT AUC (mM × min)
m
Time after insulin injection (min)
ITT AUC (mM × min)
n
Serum Insulin level (mU/L)
o
HOMA-IR Score

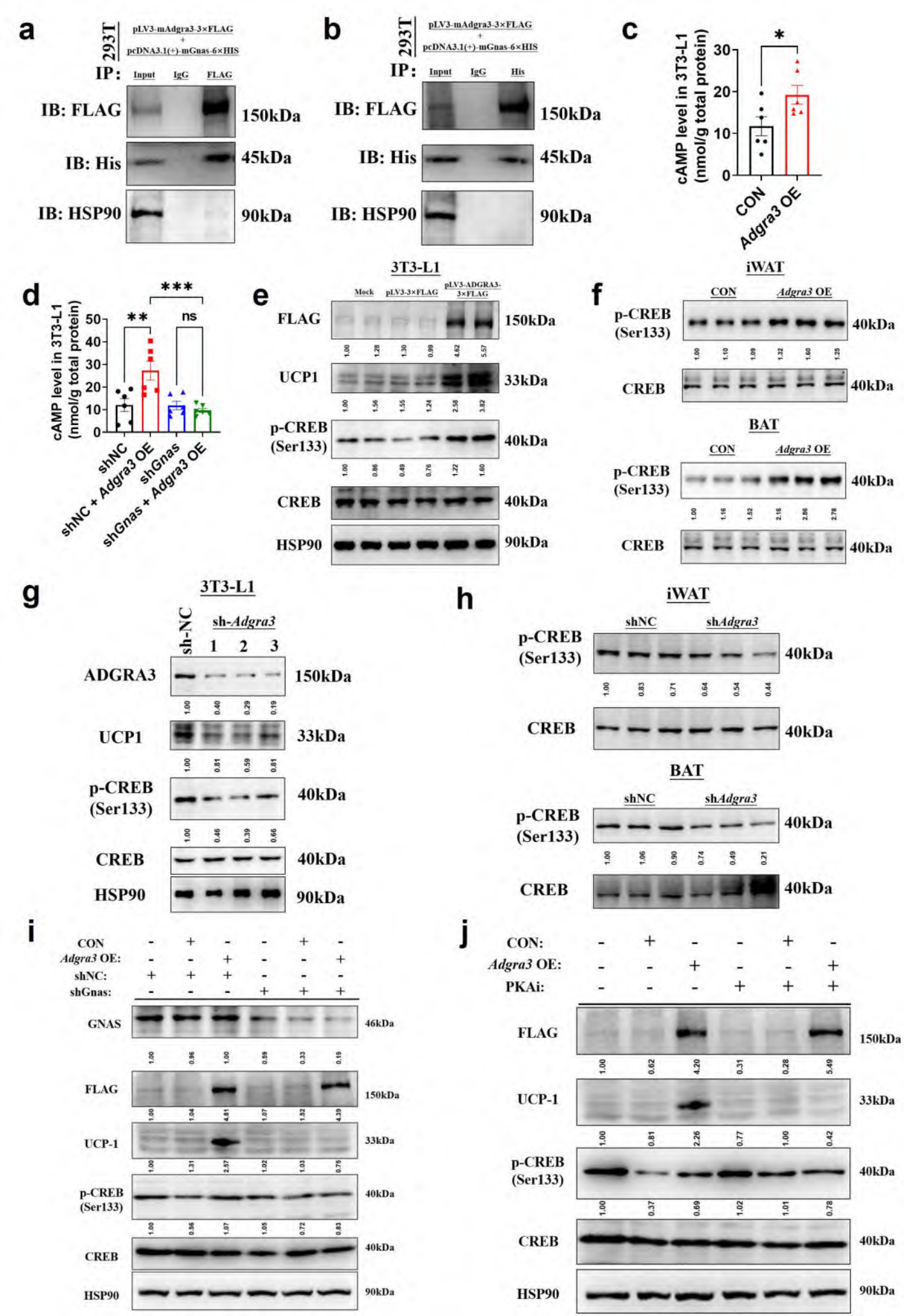
a
293T
pLV3-mAdgra3-3×FLAG
+
pcDNA3.1(+)-mGnas-6×HIS
IP:
Input
IgG
FLAG
IB: FLAG
150kDa
IB: His
45kDa
IB: HSP90
90kDa
b
293T
pLV3-mAdgra3-3×FLAG
+
pcDNA3.1(+)-mGnas-6×HIS
IP:
Input
IgG
His
IB: FLAG
150kDa
IB: His
45kDa
IB: HSP90
90kDa
c
cAMP level in 3T3-L1 (nmol/g total protein)
30
20
10
0
*
CON
Adgra3 OE
d
cAMP level in 3T3-L1 (nmol/g total protein)
50
40
30
20
10
0
**
***
ns
shNC
shNC + Adgra3 OE
shGnas
shGnas + Adgra3 OE
e
3T3-L1
Mock
pLV3-3×FLAG
pLV3-ADGRA3-3×FLAG
FLAG
150kDa
1.00
1.28
1.30
0.99
4.62
5.57
UCP1
33kDa
1.00
1.56
1.55
1.24
2.58
3.82
p-CREB (Ser133)
40kDa
1.00
0.86
0.49
0.76
1.22
1.60
CREB
40kDa
HSP90
90kDa
f
iWAT
CON
Adgra3 OE
p-CREB (Ser133)
40kDa
1.00
1.10
1.09
1.32
1.60
1.25
CREB
40kDa
BAT
CON
Adgra3 OE
p-CREB (Ser133)
40kDa
1.00
1.16
1.52
2.16
2.86
2.78
CREB
40kDa
g
3T3-L1
sh-NC
sh-Adgra3
1
2
3
ADGRA3
150kDa
1.00
0.40
0.29
0.19
UCP1
33kDa
1.00
0.81
0.59
0.81
p-CREB (Ser133)
40kDa
1.00
0.46
0.39
0.66
CREB
40kDa
HSP90
90kDa
h
iWAT
shNC
shAdgra3
p-CREB (Ser133)
40kDa
1.00
0.83
0.71
0.64
0.54
0.44
CREB
40kDa
BAT
shNC
shAdgra3
p-CREB (Ser133)
40kDa
1.00
1.06
0.90
0.74
0.49
0.21
CREB
40kDa
i
CON
Adgra3 OE:
shNC:
shGnas:
GNAS
46kDa
1.00
0.96
1.00
0.59
0.33
0.19
FLAG
150kDa
1.00
1.04
4.81
1.07
1.52
4.39
UCP-1
33kDa
1.00
1.31
2.57
1.02
1.03
0.75
p-CREB (Ser133)
40kDa
1.00
0.56
1.07
1.05
0.72
0.83
CREB
40kDa
HSP90
90kDa
j
CON:
Adgra3 OE:
PKAi:
FLAG
150kDa
1.00
0.62
4.20
0.31
0.28
5.49
UCP-1
33kDa
1.00
0.81
2.26
0.77
1.00
0.42
p-CREB (Ser133)
40kDa
1.00
0.37
0.69
1.02
1.01
0.78
CREB
40kDa
HSP90
90kDa

a

ADGRA3

Human Metabolite	Log2 Activation Fold
Hesperetin	0.7251951
D-(-)-Penicillamine	0.7243269
2-Nonanone	0.6738986
Methyl nonanoate	0.6660466
(+/-)-Propranolol HCL	0.6429146
2-Picolinic acid	0.6220501
Isoliquiritigenin	0.6157867
Isobutyric acid	0.6109246
Valeric acid	0.6043193
Octanal	0.6016749

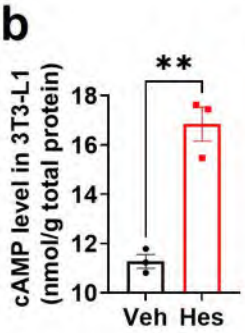

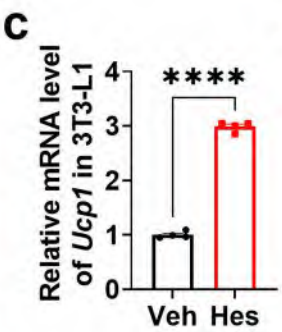

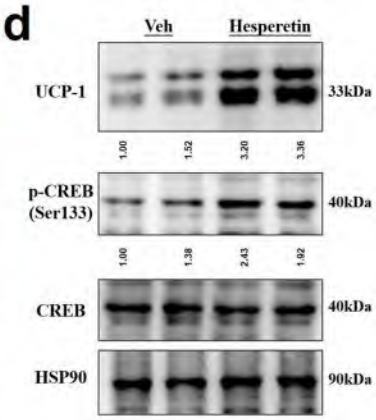

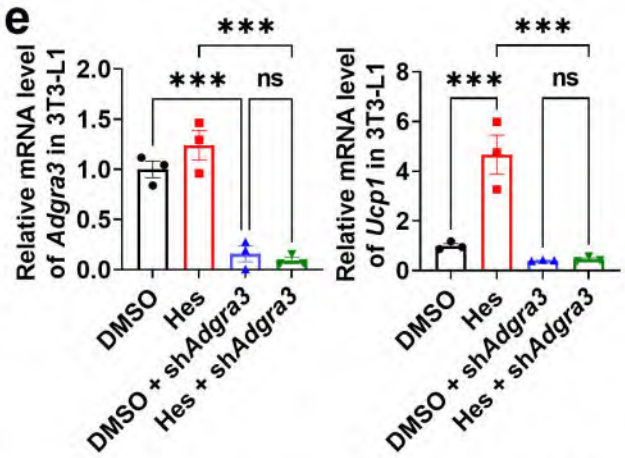

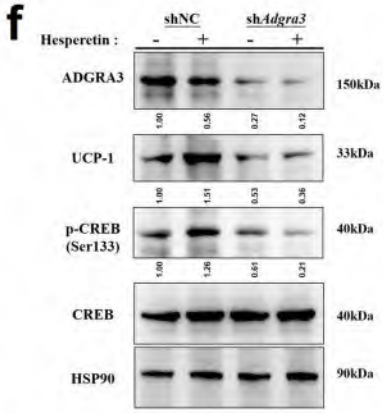

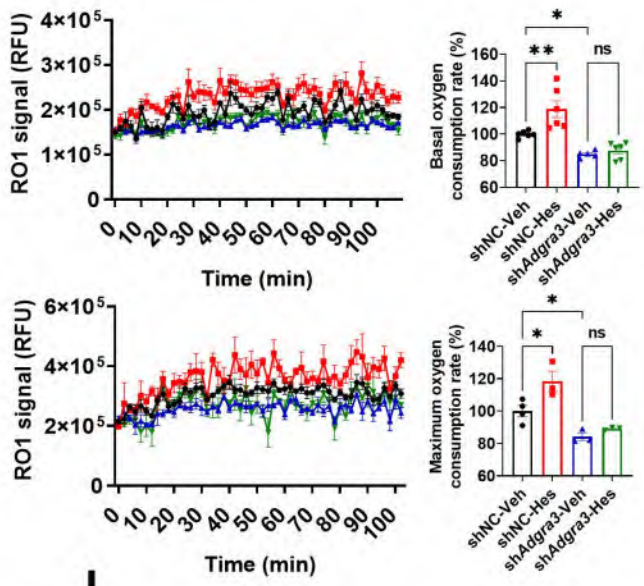

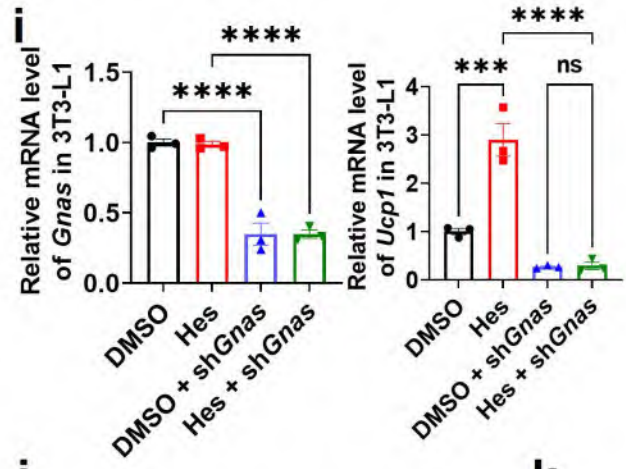

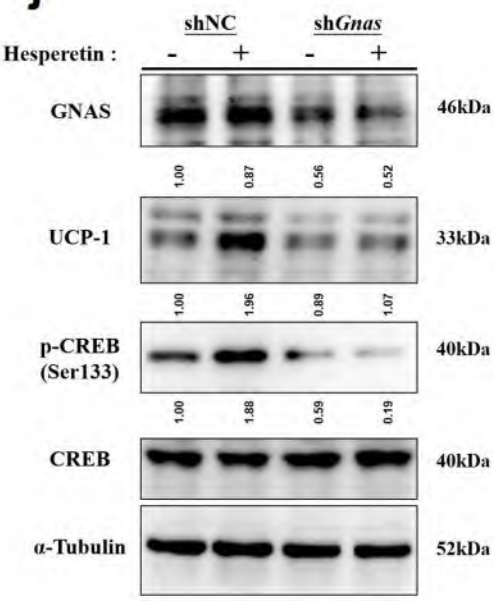

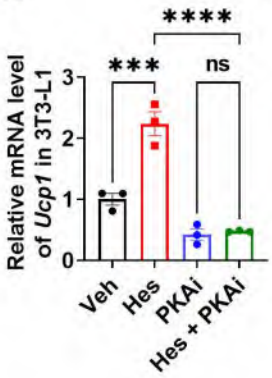

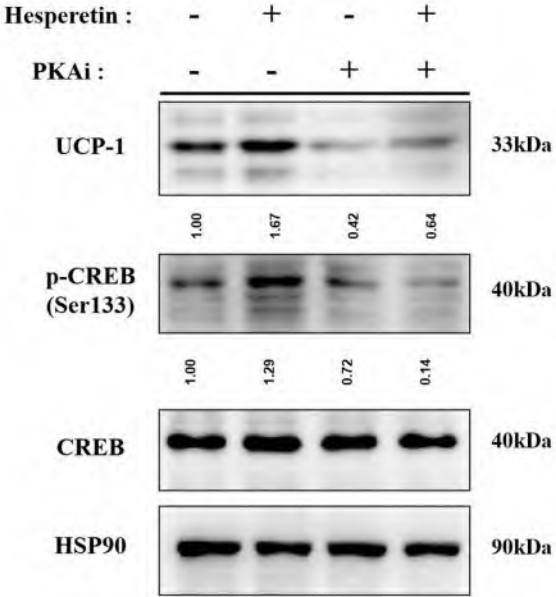

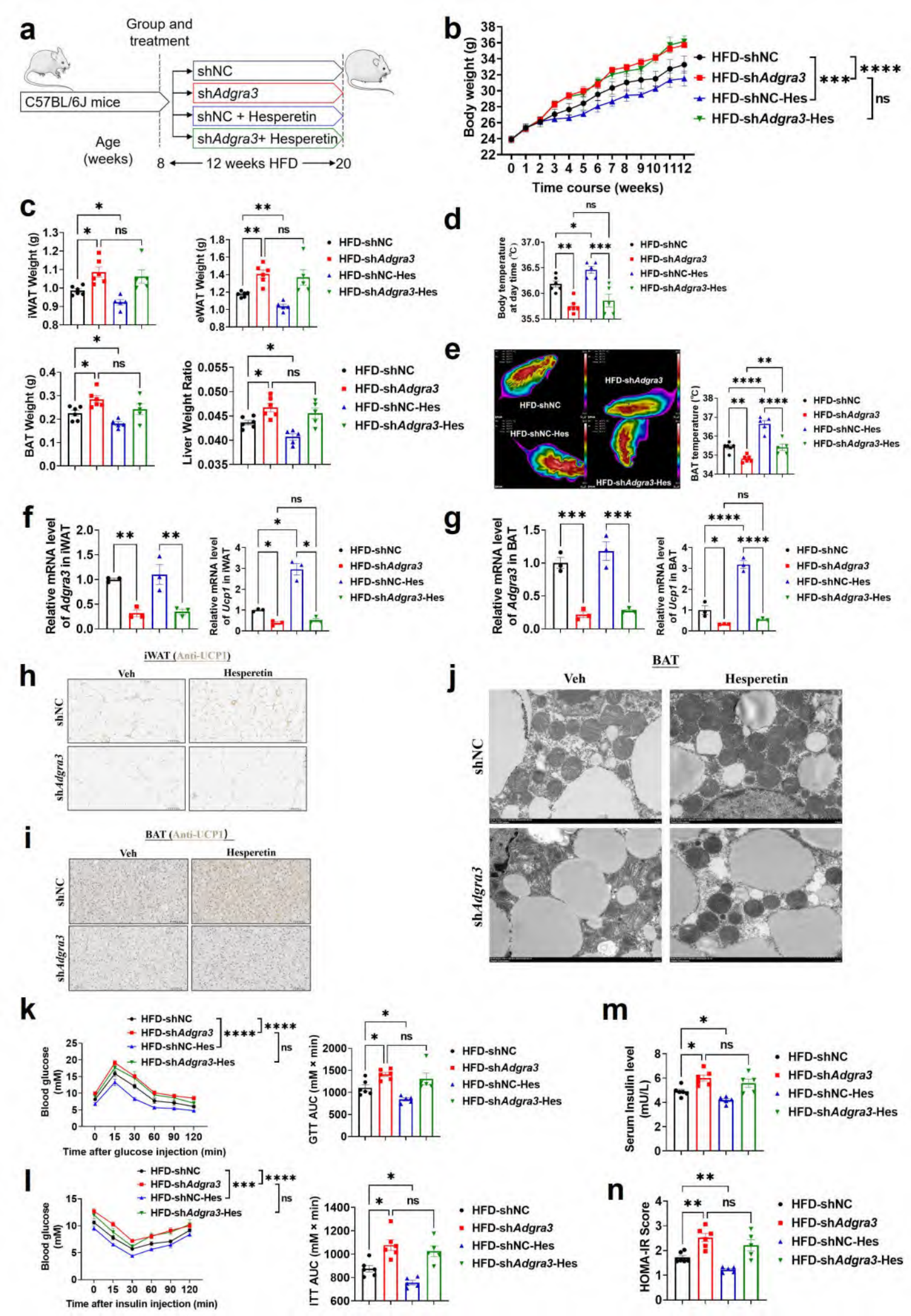
a
Group and treatment
C57BL/6J mice
shNC
shAdgra3
shNC + Hesperetin
shAdgra3+ Hesperetin
Age (weeks)
8
12 weeks HFD
20
b
Body weight (g)
Time course (weeks)
HFD-shNC
HFD-shAdgra3
HFD-shNC-Hes
HFD-shAdgra3-Hes
***
****
ns
c
iWAT Weight (g)
eWAT Weight (g)
BAT Weight (g)
Liver Weight Ratio
d
Body temperature at day time (℃)
e
HFD-shNC
HFD-shAdgra3
HFD-shNC-Hes
HFD-shAdgra3-Hes
BAT temperature (℃)
f
Relative mRNA level of Adgra3 in iWAT
Relative mRNA level of Ucp1 in iWAT
g
Relative mRNA level of Adgra3 in BAT
Relative mRNA level of Ucp1 in BAT
h
iWAT (Anti-UCP1)
Veh
Hesperetin
shNC
shAdgra3
i
BAT (Anti-UCP1)
j
BAT
k
Blood glucose (mM)
Time after glucose injection (min)
GTT AUC (mM × min)
m
Serum Insulin level (mU/L)
l
Time after insulin injection (min)
ITT AUC (mM × min)
n
HOMA-IR Score

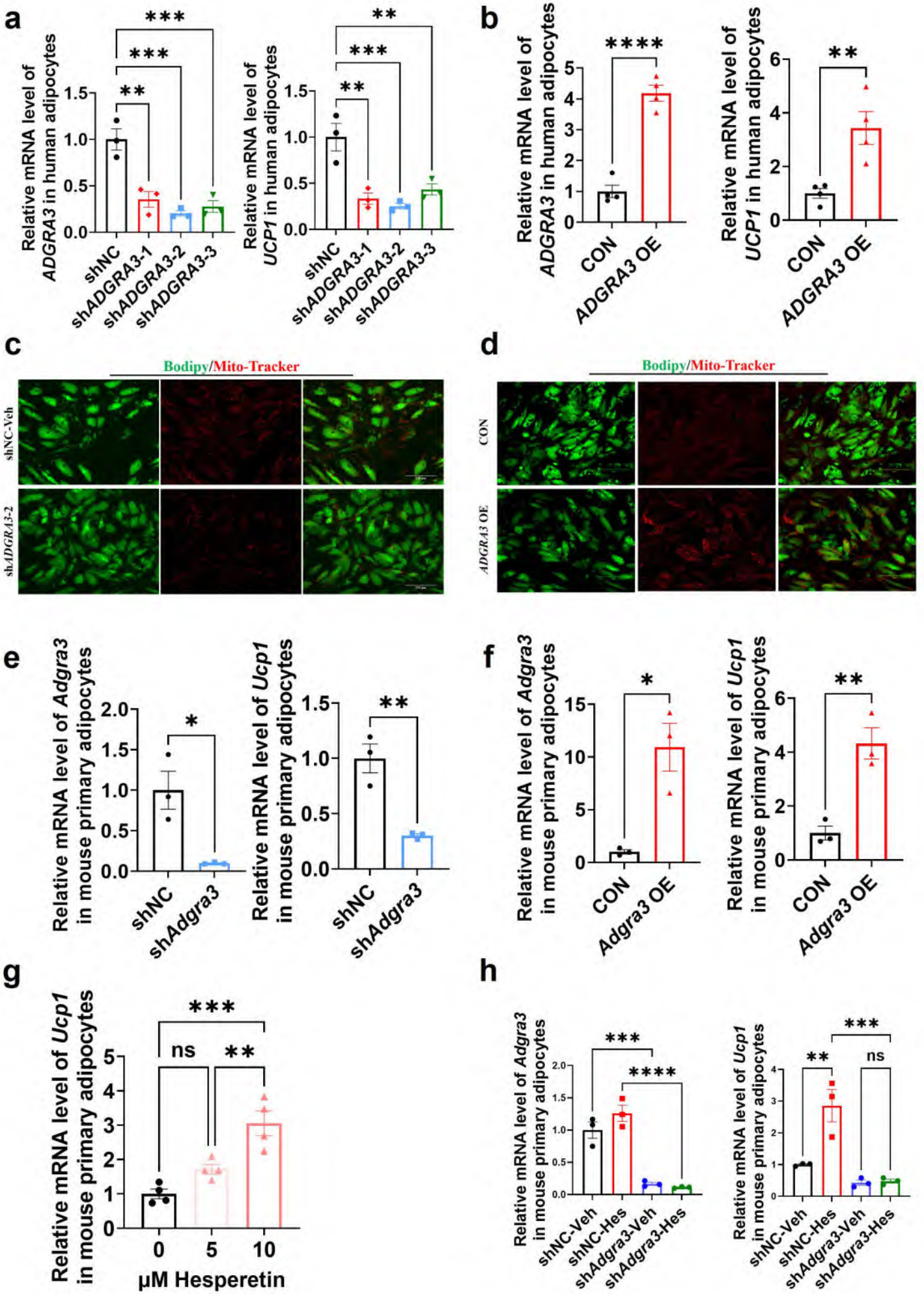
a
Relative mRNA level of ADGRA3 in human adipocytes
shNC
shADGRA3-1
shADGRA3-2
shADGRA3-3
Relative mRNA level of UCP1 in human adipocytes
b
Relative mRNA level of ADGRA3 in human adipocytes
CON
ADGRA3 OE
Relative mRNA level of UCP1 in human adipocytes
c
Bodipy/Mito-Tracker
shNC-Veh
shADGRA3-2
d
Bodipy/Mito-Tracker
CON
ADGRA3 OE
e
Relative mRNA level of Adgra3 in mouse primary adipocytes
shNC
shAdgra3
Relative mRNA level of Ucp1 in mouse primary adipocytes
f
Relative mRNA level of Adgra3 in mouse primary adipocytes
CON
Adgra3 OE
Relative mRNA level of Ucp1 in mouse primary adipocytes
g
Relative mRNA level of Ucp1 in mouse primary adipocytes
ns
0
5
10
μM Hesperetin
h
Relative mRNA level of Adgra3 in mouse primary adipocytes
shNC-Veh
shNC-Hes
shAdgra3-Veh
shAdgra3-Hes
Relative mRNA level of Ucp1 in mouse primary adipocytes

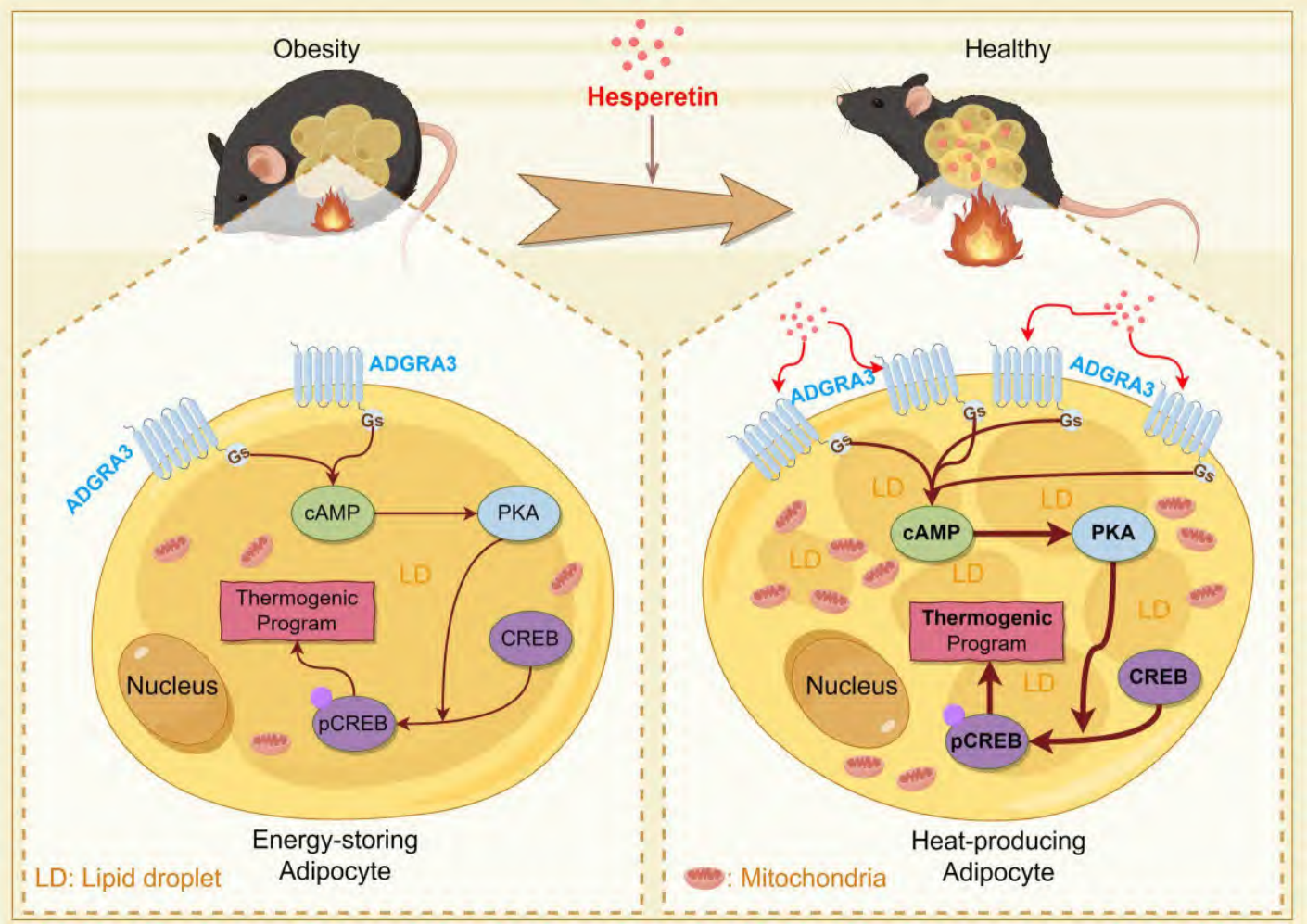
Obesity
Hesperetin
Healthy
ADGRA3
ADGRA3
Gs
Gs
cAMP
PKA
LD
Thermogenic Program
CREB
Nucleus
pCREB
Energy-storing Adipocyte
LD: Lipid droplet
ADGRA3
ADGRA3
Gs
Gs
Gs
Gs
LD
LD
cAMP
PKA
LD
LD
LD
Thermogenic Program
LD
Nucleus
CREB
pCREB
Heat-producing Adipocyte
: Mitochondria

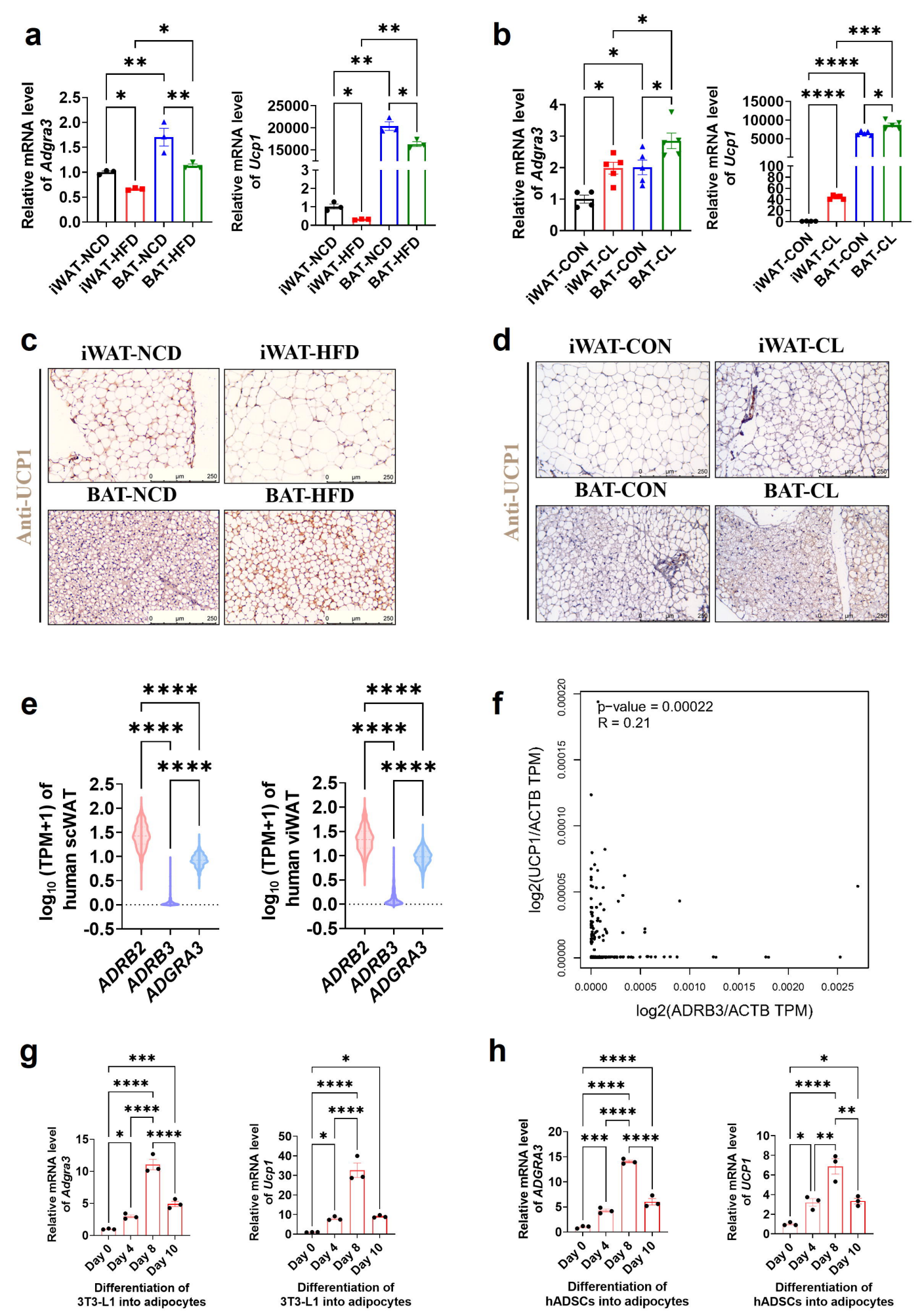
a
Relative mRNA level of Adgra3
iWAT-NCD
iWAT-HFD
BAT-NCD
BAT-HFD
Relative mRNA level of Ucp1
b
iWAT-CON
iWAT-CL
BAT-CON
BAT-CL
c
Anti-UCP1
d
e
log10 (TPM+1) of human scWAT
log10 (TPM+1) of human viWAT
ADRB2
ADRB3
ADGRA3
f
p-value = 0.00022
R = 0.21
log2(UCP1/ACTB TPM)
log2(ADRB3/ACTB TPM)
g
Relative mRNA level of Adgra3
Relative mRNA level of Ucp1
Day 0
Day 4
Day 8
Day 10
Differentiation of 3T3-L1 into adipocytes
h
Relative mRNA level of ADGRA3
Relative mRNA level of UCP1
Differentiation of hADSCs into adipocytes

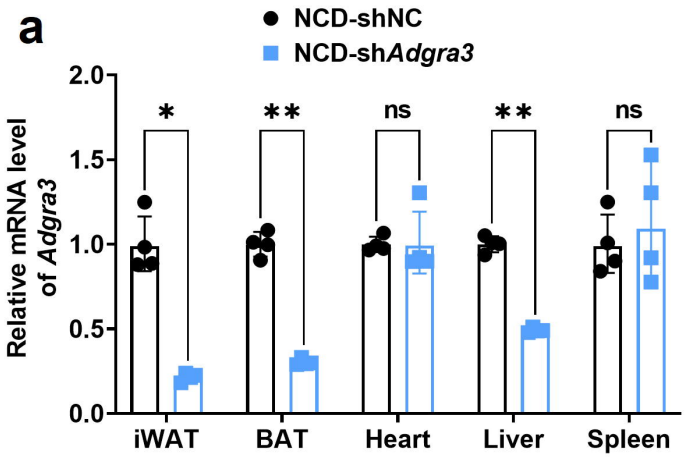
a
NCD-shNC
NCD-shAdgra3
Relative mRNA level of Adgra3
2.0
1.5
1.0
0.5
0.0
*
**
ns
**
ns
iWAT
BAT
Heart
Liver
Spleen

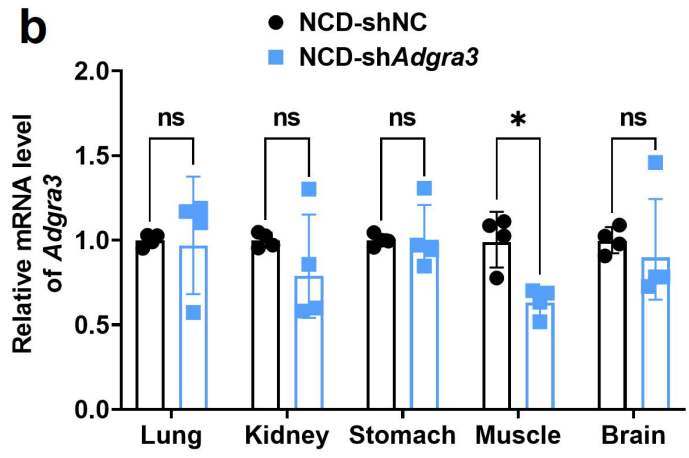
b
NCD-shNC
NCD-shAdgra3
Relative mRNA level of Adgra3
2.0
1.5
1.0
0.5
0.0
ns
ns
ns
*
ns
Lung
Kidney
Stomach
Muscle
Brain

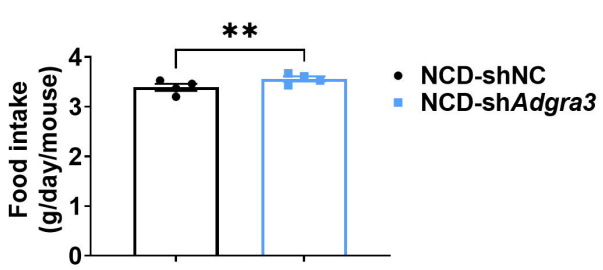
c
Food intake (g/day/mouse)
4
3
2
1
0
**
NCD-shNC
NCD-shAdgra3

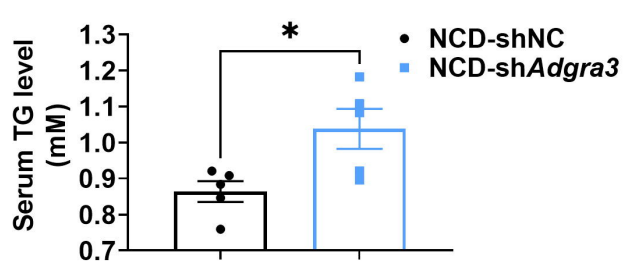
d
Serum TG level (mM)
1.3
1.2
1.1
1.0
0.9
0.8
0.7
*
NCD-shNC
NCD-shAdgra3

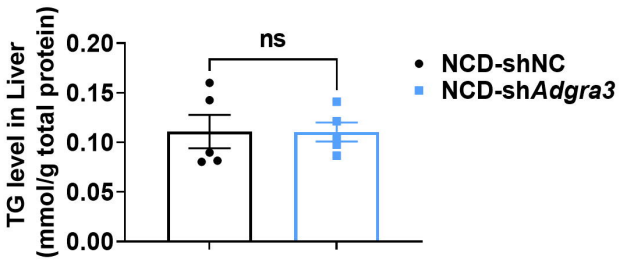
e
TG level in Liver (mmol/g total protein)
0.20
0.15
0.10
0.05
0.00
ns
NCD-shNC
NCD-shAdgra3

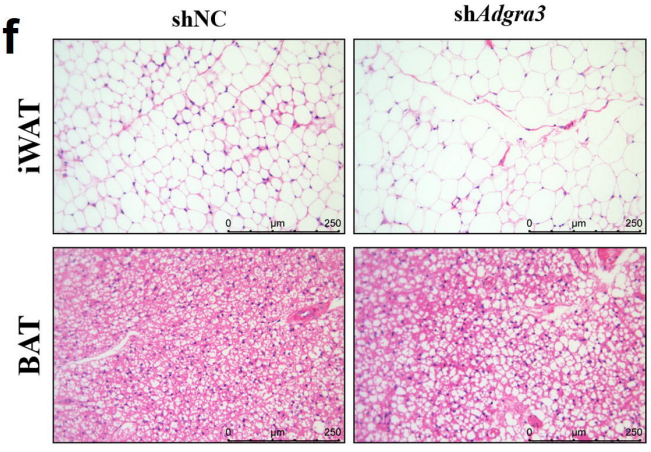
f
shNC
shAdgra3
iWAT
BAT

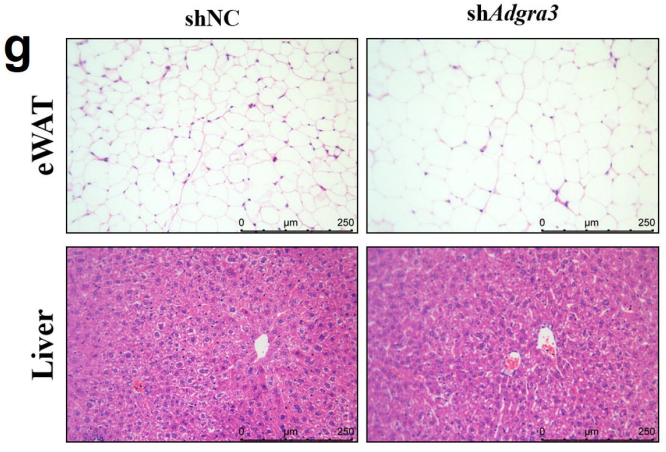
g
shNC
shAdgra3
eWAT
Liver

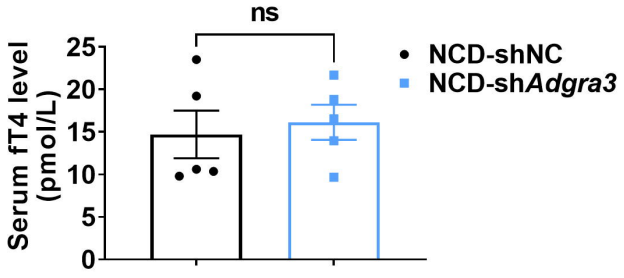
h
Serum fT4 level (pmol/L)
25
20
15
10
5
0
ns
NCD-shNC
NCD-shAdgra3

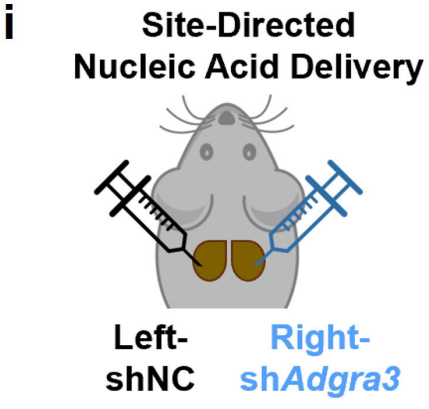
i
Site-Directed Nucleic Acid Delivery
Left-shNC
Right-shAdgra3

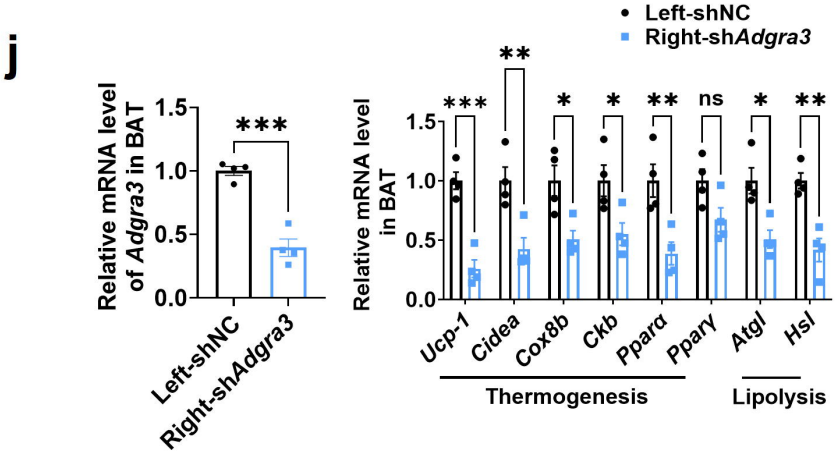
j
Left-shNC
Right-shAdgra3
Relative mRNA level of Adgra3 in BAT
1.5
1.0
0.5
0.0
***
Left-shNC
Right-shAdgra3
Relative mRNA level in BAT
***
**
*
*
**
ns
*
**
Ucp-1
Cidea
Cox8b
Ckb
Pparα
Pparγ
Atgl
Hsl
Thermogenesis
Lipolysis

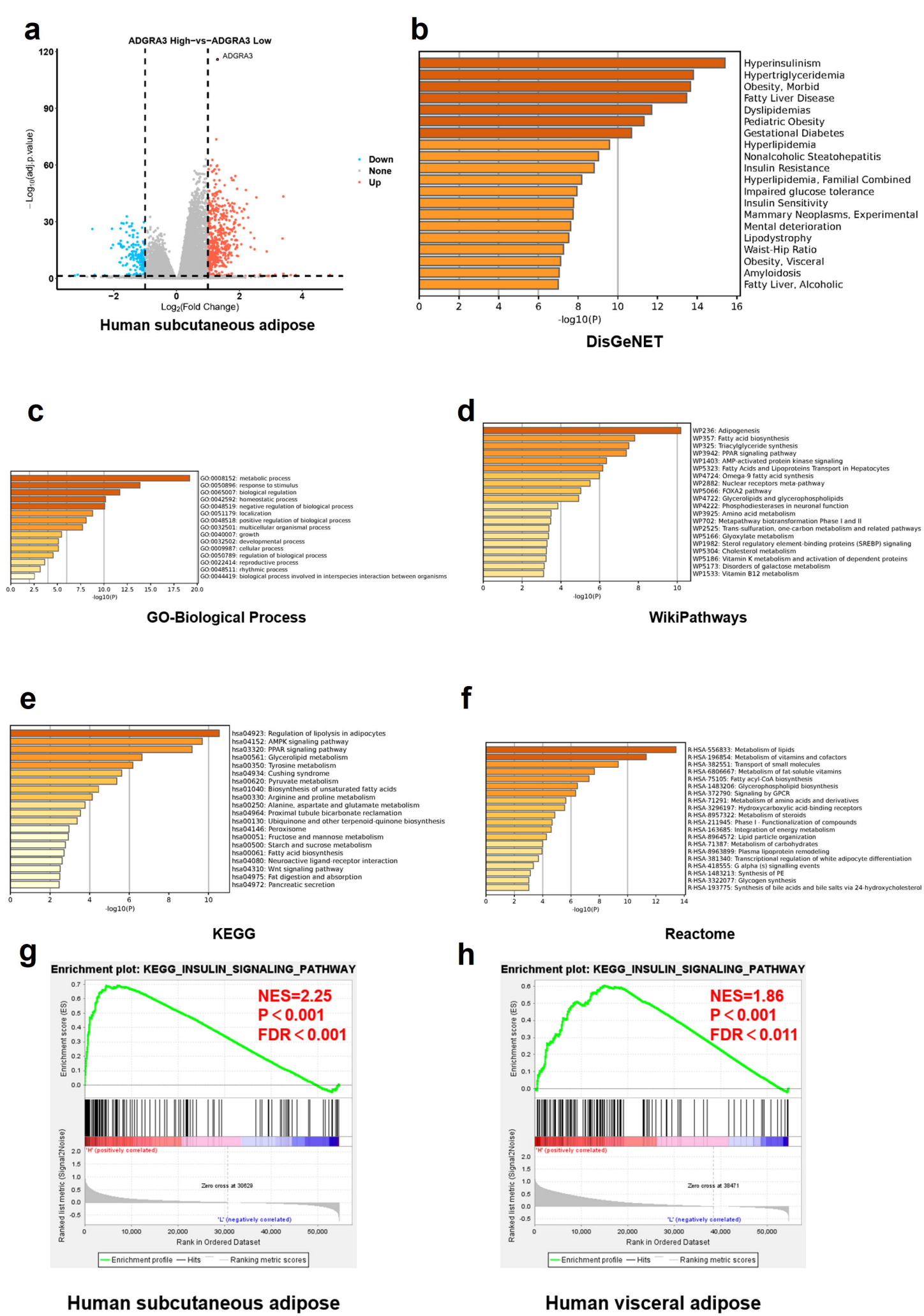
a
ADGRA3 High−vs−ADGRA3 Low
ADGRA3
−Log10(adj.p.value)
Log2(Fold Change)
Down
None
Up
Human subcutaneous adipose
b
Hyperinsulinism
Hypertriglyceridemia
Obesity, Morbid
Fatty Liver Disease
Dyslipidemias
Pediatric Obesity
Gestational Diabetes
Hyperlipidemia
Nonalcoholic Steatohepatitis
Insulin Resistance
Hyperlipidemia, Familial Combined
Impaired glucose tolerance
Insulin Sensitivity
Mammary Neoplasms, Experimental
Mental deterioration
Lipodystrophy
Waist-Hip Ratio
Obesity, Visceral
Amyloidosis
Fatty Liver, Alcoholic
-log10(P)
DisGeNET
c
GO:0008152: metabolic process
GO:0050896: response to stimulus
GO:0065007: biological regulation
GO:0042592: homeostatic process
GO:0048519: negative regulation of biological process
GO:0051179: localization
GO:0048518: positive regulation of biological process
GO:0032501: multicellular organismal process
GO:0040007: growth
GO:0032502: developmental process
GO:0009987: cellular process
GO:0050789: regulation of biological process
GO:0022414: reproductive process
GO:0048511: rhythmic process
GO:0044419: biological process involved in interspecies interaction between organisms
-log10(P)
GO-Biological Process
d
WP236: Adipogenesis
WP357: Fatty acid biosynthesis
WP325: Triacylglyceride synthesis
WP3942: PPAR signaling pathway
WP1403: AMP-activated protein kinase signaling
WP5323: Fatty Acids and Lipoproteins Transport in Hepatocytes
WP4724: Omega-9 fatty acid synthesis
WP2882: Nuclear receptors meta-pathway
WP5066: FOXA2 pathway
WP4722: Glycerolipids and glycerophospholipids
WP4222: Phosphodiesterases in neuronal function
WP3925: Amino acid metabolism
WP702: Metapathway biotransformation Phase I and II
WP2525: Trans-sulfuration, one-carbon metabolism and related pathways
WP5166: Glyoxylate metabolism
WP1982: Sterol regulatory element-binding proteins (SREBP) signaling
WP5304: Cholesterol metabolism
WP5186: Vitamin K metabolism and activation of dependent proteins
WP5173: Disorders of galactose metabolism
WP1533: Vitamin B12 metabolism
-log10(P)
WikiPathways
e
hsa04923: Regulation of lipolysis in adipocytes
hsa04152: AMPK signaling pathway
hsa03320: PPAR signaling pathway
hsa00561: Glycerolipid metabolism
hsa00350: Tyrosine metabolism
hsa04934: Cushing syndrome
hsa00620: Pyruvate metabolism
hsa01040: Biosynthesis of unsaturated fatty acids
hsa00330: Arginine and proline metabolism
hsa00250: Alanine, aspartate and glutamate metabolism
hsa04964: Proximal tubule bicarbonate reclamation
hsa00130: Ubiquinone and other terpenoid-quinone biosynthesis
hsa04146: Peroxisome
hsa00051: Fructose and mannose metabolism
hsa00500: Starch and sucrose metabolism
hsa00061: Fatty acid biosynthesis
hsa04080: Neuroactive ligand-receptor interaction
hsa04310: Wnt signaling pathway
hsa04975: Fat digestion and absorption
hsa04972: Pancreatic secretion
-log10(P)
KEGG
f
R-HSA-556833: Metabolism of lipids
R-HSA-196854: Metabolism of vitamins and cofactors
R-HSA-382551: Transport of small molecules
R-HSA-6806667: Metabolism of fat-soluble vitamins
R-HSA-75105: Fatty acyl-CoA biosynthesis
R-HSA-1483206: Glycerophospholipid biosynthesis
R-HSA-372790: Signaling by GPCR
R-HSA-71291: Metabolism of amino acids and derivatives
R-HSA-3296197: Hydroxycarboxylic acid-binding receptors
R-HSA-8957322: Metabolism of steroids
R-HSA-211945: Phase I - Functionalization of compounds
R-HSA-163685: Integration of energy metabolism
R-HSA-8964572: Lipid particle organization
R-HSA-71387: Metabolism of carbohydrates
R-HSA-8963899: Plasma lipoprotein remodeling
R-HSA-381340: Transcriptional regulation of white adipocyte differentiation
R-HSA-418555: G alpha (s) signalling events
R-HSA-1483213: Synthesis of PE
R-HSA-3322077: Glycogen synthesis
R-HSA-193775: Synthesis of bile acids and bile salts via 24-hydroxycholesterol
-log10(P)
Reactome
g
Enrichment plot: KEGG_INSULIN_SIGNALING_PATHWAY
NES=2.25
P < 0.001
FDR < 0.001
Enrichment score (ES)
'H' (positively correlated)
Zero cross at 30629
'L' (negatively correlated)
Ranked list metric (Signal2Noise)
Rank in Ordered Dataset
Enrichment profile
Hits
Ranking metric scores
Human subcutaneous adipose
h
Enrichment plot: KEGG_INSULIN_SIGNALING_PATHWAY
NES=1.86
P < 0.001
FDR < 0.011
Enrichment score (ES)
'H' (positively correlated)
Zero cross at 38471
'L' (negatively correlated)
Ranked list metric (Signal2Noise)
Rank in Ordered Dataset
Enrichment profile
Hits
Ranking metric scores
Human visceral adipose

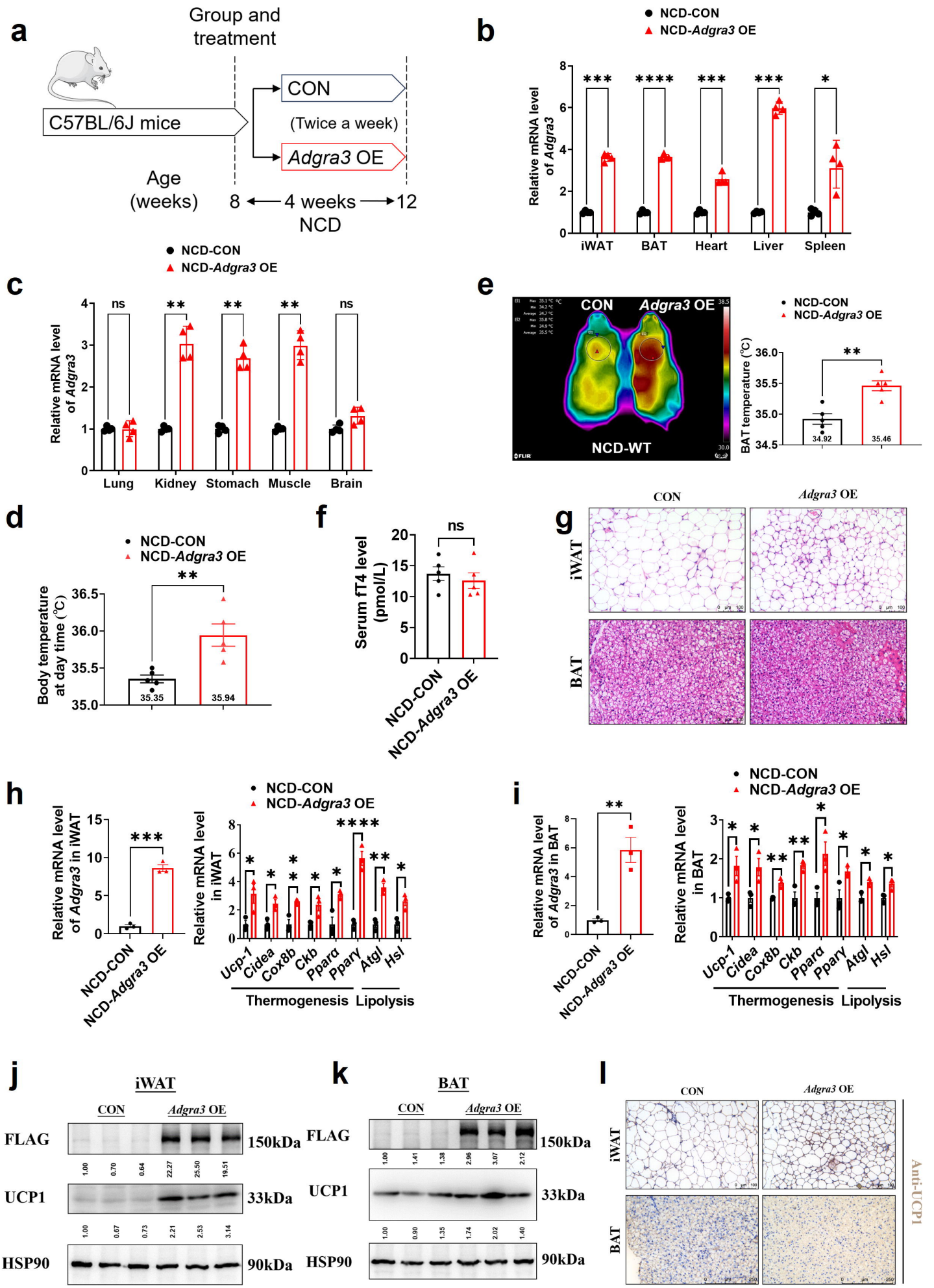
a
Group and treatment
C57BL/6J mice
CON
(Twice a week)
Adgra3 OE
Age (weeks)
8
4 weeks NCD
12
b
NCD-CON
NCD-Adgra3 OE
Relative mRNA level of Adgra3
iWAT
BAT
Heart
Liver
Spleen
c
Relative mRNA level of Adgra3
Lung
Kidney
Stomach
Muscle
Brain
ns
d
Body temperature at day time (℃)
35.35
35.94
e
CON
Adgra3 OE
NCD-WT
BAT temperature (℃)
34.92
35.46
f
Serum fT4 level (pmol/L)
NCD-CON
NCD-Adgra3 OE
g
CON
Adgra3 OE
iWAT
BAT
h
Relative mRNA level of Adgra3 in iWAT
Relative mRNA level in iWAT
Ucp-1
Cidea
Cox8b
Ckb
Pparα
Pparγ
Atgl
Hsl
Thermogenesis
Lipolysis
i
Relative mRNA level of Adgra3 in BAT
Relative mRNA level in BAT
j
iWAT
FLAG
UCP1
HSP90
150kDa
33kDa
90kDa
k
BAT
l
Anti-UCP1

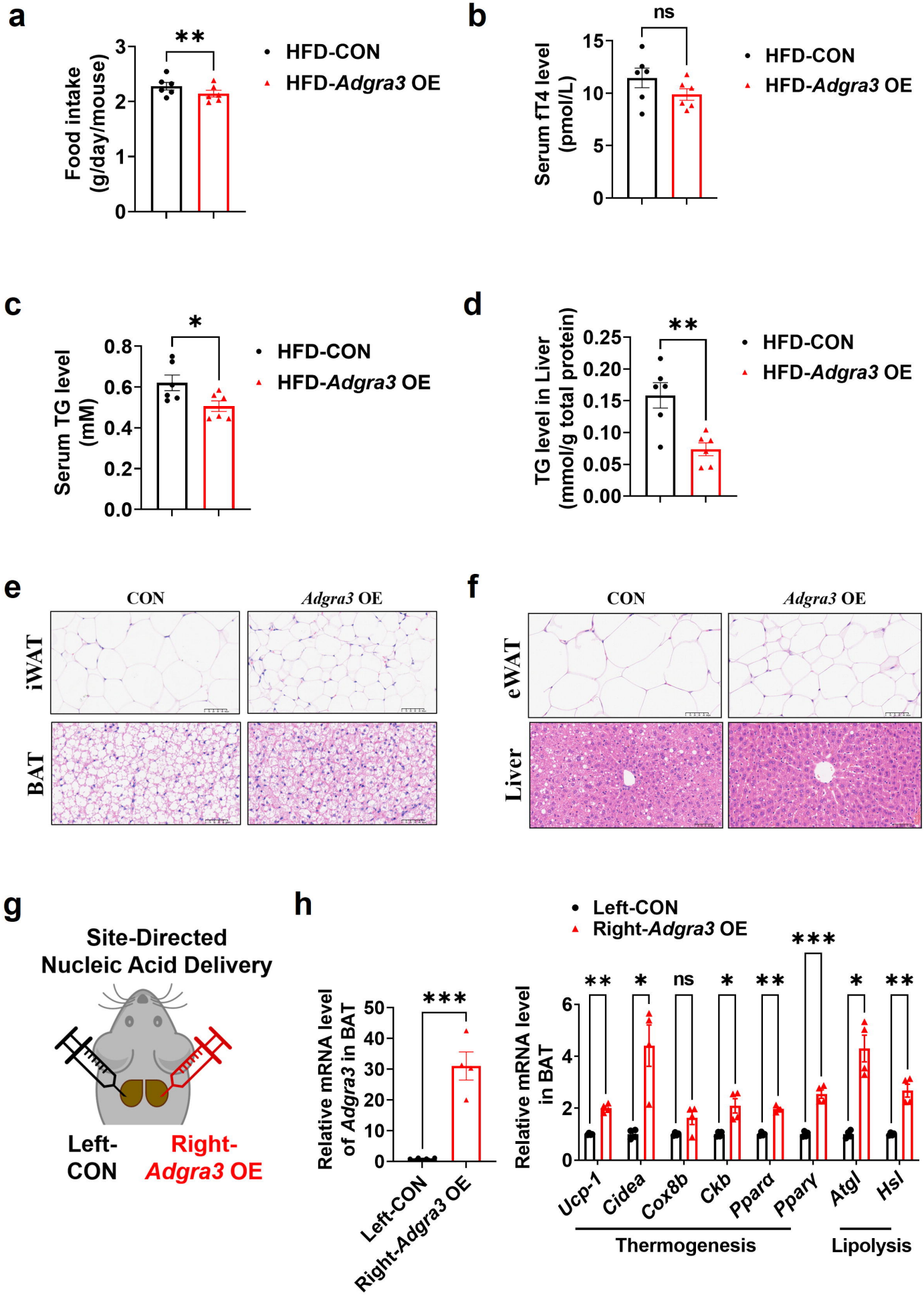
a
Food intake (g/day/mouse)
**
HFD-CON
HFD-Adgra3 OE
b
Serum fT4 level (pmol/L)
ns
HFD-CON
HFD-Adgra3 OE
c
Serum TG level (mM)
*
HFD-CON
HFD-Adgra3 OE
d
TG level in Liver (mmol/g total protein)
**
HFD-CON
HFD-Adgra3 OE
e
CON
Adgra3 OE
iWAT
BAT
f
CON
Adgra3 OE
eWAT
Liver
g
Site-Directed Nucleic Acid Delivery
Left-CON
Right-Adgra3 OE
h
Left-CON
Right-Adgra3 OE
Relative mRNA level of Adgra3 in BAT
***
Left-CON
Right-Adgra3 OE
Relative mRNA level in BAT
** * ns * ** *** * **
Ucp-1
Cidea
Cox8b
Ckb
Pparα
Pparγ
Atgl
Hsl
Thermogenesis
Lipolysis

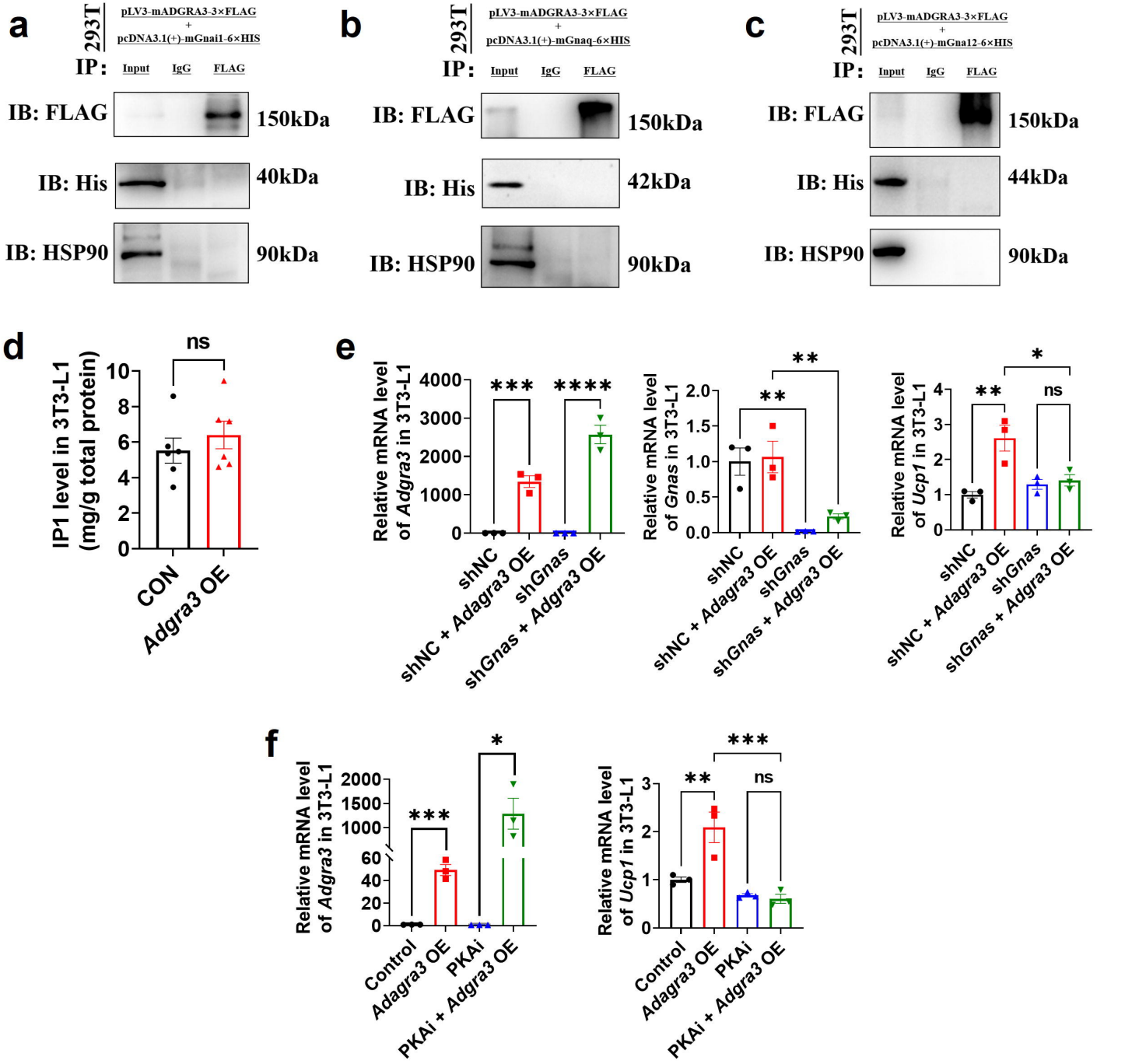
a
293T
pLV3-mADGRA3-3×FLAG
+
pcDNA3.1(+)-mGnai1-6×HIS
IP:
Input
IgG
FLAG
IB: FLAG
150kDa
IB: His
40kDa
IB: HSP90
90kDa
b
293T
pLV3-mADGRA3-3×FLAG
+
pcDNA3.1(+)-mGnaq-6×HIS
IP:
Input
IgG
FLAG
IB: FLAG
150kDa
IB: His
42kDa
IB: HSP90
90kDa
c
293T
pLV3-mADGRA3-3×FLAG
+
pcDNA3.1(+)-mGna12-6×HIS
IP:
Input
IgG
FLAG
IB: FLAG
150kDa
IB: His
44kDa
IB: HSP90
90kDa
d
IP1 level in 3T3-L1 (mg/g total protein)
ns
CON
Adgra3 OE
e
Relative mRNA level of Adgra3 in 3T3-L1
***
****
Relative mRNA level of Gnas in 3T3-L1
**
**
Relative mRNA level of Ucp1 in 3T3-L1
**
ns
*
shNC
shNC + Adagra3 OE
shGnas
shGnas + Adgra3 OE
f
Relative mRNA level of Adgra3 in 3T3-L1
***
*
Relative mRNA level of Ucp1 in 3T3-L1
**
ns
***
Control
Adagra3 OE
PKAi
PKAi + Adgra3 OE

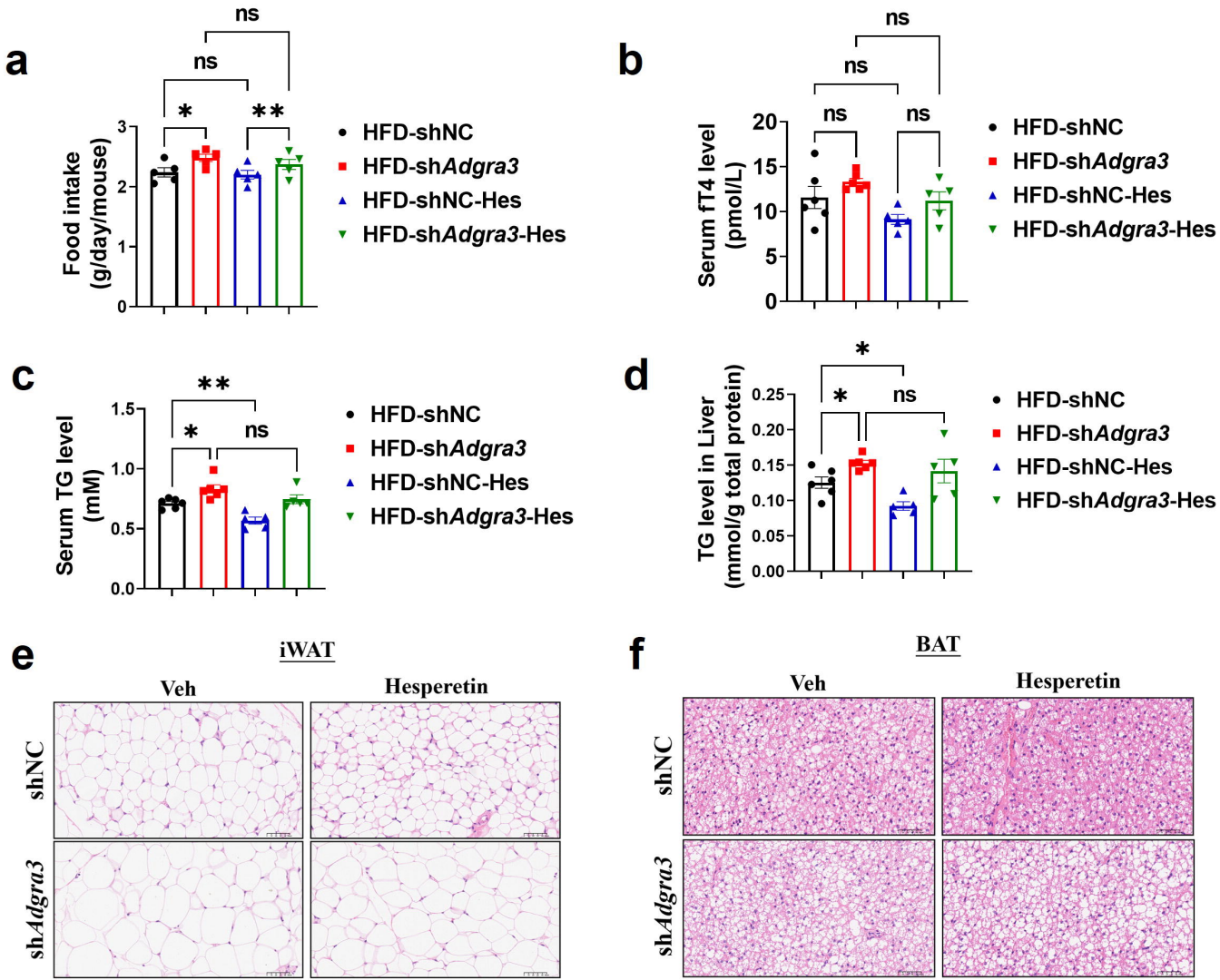
a
ns
ns
*
**
Food intake (g/day/mouse)
3
2
1
0
HFD-shNC
HFD-shAdgra3
HFD-shNC-Hes
HFD-shAdgra3-Hes
b
ns
ns
ns
ns
Serum fT4 level (pmol/L)
20
15
10
5
0
HFD-shNC
HFD-shAdgra3
HFD-shNC-Hes
HFD-shAdgra3-Hes
c
**
*
ns
Serum TG level (mM)
1.5
1.0
0.5
0.0
HFD-shNC
HFD-shAdgra3
HFD-shNC-Hes
HFD-shAdgra3-Hes
d
*
*
ns
TG level in Liver (mmol/g total protein)
0.25
0.20
0.15
0.10
0.05
0.00
HFD-shNC
HFD-shAdgra3
HFD-shNC-Hes
HFD-shAdgra3-Hes
e
iWAT
Veh
Hesperetin
shNC
shAdgra3
f
BAT
Veh
Hesperetin
shNC
shAdgra3